

Jana Daxnerová

Hydraulic Scale Modelling of Flow Calming Structures for Hydropower Plants

April 2019



Norwegian University of
Science and Technology

Hydraulic Scale Modelling of Flow Calming Structures for Hydropower Plants

Jana Daxnerová

Hydropower Development

Submission date: April 2019

Supervisor: Kaspar Vatland Vereide

Co-supervisor: Ola Haugen Havrevoll
Leif Lia

Norwegian University of Science and Technology
Department of Civil and Environmental Engineering

Abstract

Several large hydropower plants in Norway have been upgraded with a higher installed capacity, but unfortunately, this upgrade has also brought with it operational problems because of sediments entering penstock and causing damage to the turbine. This was due to a sand trap which was not functioning as projected after the upgrade. To improve sand trap efficiency, several proposals were considered. One of them was to calm and homogenize the flow by using a flow calming structure.

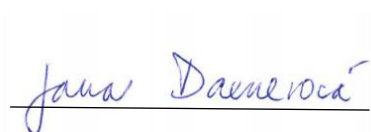
The main objective of this thesis was to propose the optimum design of a sand trap flow calming structure for Tonstad hydropower plant, which was one of the hydropower plants facing operational problems after an upgrade. To find the optimum designed of such a structure, three different flow calming structures were designed, constructed in the model scale, tested in the hydraulic scale model and compared to each other.

The results showed that the implementation of flow calming structure improved sand trap efficiency. All three flow calming structures provided very similar, satisfactory, results. Sand trap efficiency increased from 95.67 % to more than 99 %, sedimentation began already in the diffuser and occurred mainly in the upstream half of the sand trap. In terms of headloss were the results various. While flow calming structure No. 3, layout 3, increased sand trap efficiency to 99.96 % with a small headloss of 3.83 mm, flow calming structure No. 2 reached sand trap efficiency of 99.19 % with the headloss 5.2 times higher equal to 19,89 mm. This made flow calming structure No. 3 the one to be recommended for further testing and possibly installation in sand trap 3 in Tonstad HPP.

Preface

This master thesis was written at the Norwegian University of Science and Technology (NTNU), Department of Civil and Environmental Engineering (IBM) with Adjunct Associate Professor Kaspar Vereide as main supervisor and Ola Haugen Havrevoll as co-supervisor. The study presented in this thesis is a part of a bigger research project focused on improvements of sand trap 3 of Tonstad hydropower plant cooperated between IBM and Sira-Kvina power company.

Trondheim, 30.4. 2019



Jana Daxnerová

Acknowledgement

I would like to thank various people for their contribution to this study. First of all, I would like to express my deep gratitude to my supervisor Kaspar Vereide for guiding me with his valuable and constructive suggestions during this work. Big thanks for letting me be part of this research project and giving me the opportunity to work in the hydraulic laboratory. Similar appreciation is given to my co-supervisor Ola Haugen Havrevoll for his support and guidance during the literature study.

Thanks to my family and friends for their moral support over the years.

A special thanks to Geir Tesaker and Eirik Nygård for their help with the construction of flow calming structures and many theoretical and enjoyable discussions.

Last but not least I would like to thank the administrative staff at the department and my fellow students for making my study at NTNU a memorable period of life.

Table of content

Abstract	i
Preface	iii
Acknowledgement	v
Table of content	vii
List of figures	ix
List of tables	xiii
Abbreviations	xv
1 Introduction	1
1.1 <i>Background</i>	1
1.2 <i>Research objectives</i>	2
1.3 <i>Thesis structure</i>	2
2 Literature review	3
3 Theory	5
3.1 <i>General hydraulics</i>	5
3.1.1 Continuity equation	5
3.1.2 Bernoulli's principle	5
3.1.3 Energy losses	6
3.2 <i>Erosion, sediment transport, and deposition</i>	7
3.2.1 Erosion.....	7
3.2.2 Mass transport	9
3.2.3 Deposition	10
3.3 <i>Dimensional analysis and similitude</i>	10
3.4 <i>Hydraulic scale modelling</i>	11
3.4.1 Reynolds' scaling law	12
3.4.2 Froude's scaling law.....	12
4 Research methods	15
4.1 <i>Description of the prototype</i>	15
4.2 <i>Description of the hydraulic scale model</i>	17
4.2.1 Instrumentation and measurements	18
4.3 <i>Description of the experimental flume used for experiments</i>	18
4.3.1 Instrumentation and measurements	23
4.3.2 Running of the experiments.....	23
4.4 <i>Design of flow calming structures</i>	25
4.4.1 Flow calming structure No. 1	25
4.4.2 Flow calming structure No. 2.....	26

Table of content

- 4.4.3 Flow calming structure No. 328
- 5 Results 33**
 - 5.1.1 No flow calming structure33
 - 5.1.2 Flow calming structure No. 135
 - 5.1.3 Flow calming structure No. 238
 - 5.1.4 Flow calming structure No. 339
 - 5.1.5 Comparison of different designs42
- 6 Discussion 45**
 - 6.1 *Limitation of the study*46
- 7 Conclusions 49**
 - 7.1 *Suggestions for future work*.....49
- 8 References..... 51**
- 9 Appendices..... 53**
 - Appendix A: Drawings of the prototype*54

List of figures

Figure 1 Tranquilizing rack for use in an experimental flume (Open channel flow; Tracom fiberglass products).....	3
Figure 2 Three rows of tranquilizing racks (Paschmann et al., 2017).....	4
Figure 3 Processes of erosion, mass transport and sedimentation (Julien, 2010)	7
Figure 4 Shields' diagram for start of motion (Lysne et al., 2003).....	9
Figure 5 Different modes of sediment transport (Dey, 2014)	10
Figure 6 System of sand traps of Tonstad HPP (modified after Brevik, 2013)	15
Figure 7 Cross-section of the sand trap	16
Figure 8 Drawing of the hydraulic scale model of Tonstad HPP.....	17
Figure 9 Cross-section of sandtrap model	18
Figure 10 Setup of the experimental flume.....	19
Figure 11 Honeycomb installed most upstream in the flume ensuring stable inflow conditions.....	20
Figure 12 Provisional diffuser with a vibrating dosing machine.....	20
Figure 13 Weir creating the end of the sand trap (view from the upstream on the left side, side view on the right side)	20
Figure 14 Filter placed most downstream in the flume	21
Figure 15 Particle size distribution of the sand used in the experiments.....	22
Figure 16 Acoustic Doppler velocimeter installed in the flume.....	23
Figure 17 Flow calming structure used in hydraulic flumes	25
Figure 18 Design of flow calming structure No. 1.....	26
Figure 19 Photo of flow calming structure No. 1	26
Figure 20 Flow calming structure used in small hydraulic models.....	27
Figure 21 Design of flow calming structure No. 2, view from downstream	27
Figure 22 Photo of flow calming structure No. 2	28
Figure 23 Flow calming structure used in a sand trap in Germany (SITEC).....	28

List of figures

Figure 24 Design of flow calming structure No. 3, side view 29

Figure 25 Design of flow calming structure No. 3, top view..... 29

Figure 26 Photo of flow calming structure No. 3, layout 1 30

Figure 27 Photo of flow calming structure No. 3, layout 2 30

Figure 28 Photo of flow calming structure No. 3, layout 3 31

Figure 29 Results from test 1 (on the left side) and test 2 (on the right side) (view from upstream) 34

Figure 30 Detail of ripple marks developed during test 1 (on the left side) and test 2 (on the right side) (view from upstream)..... 34

Figure 31 Particle size distribution of sediments collected downstream of the sand trap 35

Figure 32 Results from test 3 (on the left side) and test 4 (on the right side) (view from upstream) 36

Figure 33 Detail of flow calming structure No. 1 after test 4 36

Figure 34 Particle size distribution of sediments collected downstream of the sand trap 37

Figure 35 Results from test 5 (on the left side) and test 6 (on the right side) (view from upstream) 38

Figure 36 Side view of the sediment’s deposition upstream and downstream of the flow calming structure (test 5 on the left side and test 6 on the right side) 39

Figure 37 Particle size distribution of sediments collected downstream of the sand trap 39

Figure 38 Results from test 7 (view from upstream)..... 40

Figure 39 Side view of the sediment’s deposition in test 7 40

Figure 40 Results from test 8 (on the left side) and test 9 (on the right side) (view from upstream) 41

Figure 41 Side view of the sediment’s deposition (test 8 on the left side and test 9 on the right side) 41

Figure 42 Relationship between sand trap efficiency and headloss caused by flow calming structure	43
Figure 43 Detail of flow calming structures during the experiments	47
Figure 44 Detail of the concrete bed of experimental flume	48

List of tables

Table 1 Overview of the tests done in the experimental flume.....	33
Table 2 Overview of results of sand trap efficiency.....	42
Table 3 Overview of results of headloss.....	42

Abbreviations

ADV	Acoustic Doppler Velocimetry
HPP	Hydroelectric Power Plant
IBM	Department of Civil and Environmental Engineering
MID	Magnetic Inductive Discharge meter
NTH	Technical University of Norway
NTNU	Norwegian University of Science and Technology
PMMA	Poly-Methyl MethAcrylate

1 Introduction

1.1 Background

The beginning of human civilization is defined by the use of energy. From the prehistoric people using fire for cooking and heating, the human civilization has evolved to the point when the consumption of energy is necessary for the functioning of the modern society and the survival of our civilization (Michaelides, 2012). In the 20th century, fossil fuels offered great opportunities for the development of society, but nowadays, we have to face the problem with gradually decreasing reserves of fossil fuels, which cannot fulfil constantly increasing demand for energy, and the negative effects of their continued use, such as greenhouse gases causing global warming and pollution that threatens human health (Armaroli & Balzani, 2007). To minimize negative environmental impacts, renewable energy sources such as hydropower, biomass, geothermal, solar, wind and marine energy, are considered as a suitable alternative to conventional fossil fuels (Bilgen, Kaygusuz, & Sari, 2004; Dincer, 2001).

Renewable energy sources have gained great attention in the last decades. New developments in these technologies have led to cost reductions and encourage utilities to expand wind and solar power capacity (Patel, 2005). Since wind and solar power plants do not provide a stable electricity output, it is necessary to ensure the balancing of energy production and production of peak power. For this purpose, hydroelectric power plants (HPP) are most suitable.

In Norway, most of the hydropower plants were built between the 1950s and the end of 1980s and the state of the installed mechanical and electrical equipment make it relevant to refurbish and upgrade these powerplants with increased efficiency and capacity of the powerplants. Upgrading of existing hydropower plants also has a smaller environmental impact than a building of new powerplants (Killingtveit, 2019; Lia, Jensen, Stensby, Midttomme, & Ruud, 2015).

Several large hydropower plants have already been upgraded with a higher installed capacity, but unfortunately, this upgrade has also brought with it problems with sediments that have not been trapped in a sand trap and have caused damage on the turbines. The reason for these problems can be that increasing of installed capacity increases also maximum discharge in an original sand trap which is not functioning as

projected after the upgrade. One of the hydropower plants which has experienced problems after an upgrade is Tonstad hydropower plant located in southern Norway. In 1988, the installed capacity of this powerplant was increased by 50%, and after this major upgrade, among other problems, flushing of sediments from a sand trap to the turbines has occurred. Damaged turbines had to be repaired, but no reconstruction has been undertaken. Nowadays, there is an effort to prevent further problems by restricting the operation of the power plant (Vereide, Svingen, & Guddal, 2015).

To understand the hydraulic behavior in sand traps, hydraulic scale models are very valuable. Therefore, a new hydraulic scale model of the sand trap 3 of Tonstad hydropower plant has been constructed at the Norwegian University of Science and Technology (NTNU).

1.2 Research objectives

The main objective of the research conducted in this master thesis is to propose the optimum design of a sand trap flow calming structure for Tonstad hydropower plant. To achieve this goal the following steps are necessary. First, a literature study of flow calming structures and the use of flow calming structures in hydropower sand traps will be carried out. Based on the available literature, three different flow calming structures will be designed, constructed in the model scale, tested in the hydraulic scale model and compared to each other.

1.3 Thesis structure

This thesis is composed of seven main chapters. Chapter 1 has presented background for this master thesis and an introduction to the work. A literature review flow calming structures research is contained in Chapter 2. Chapter 3 contains the theory behind general hydraulics in both, pressurized and open channel flow, followed by sediment transport and erosion theory. Lastly, the theory behind hydraulic scale modelling is presented. Chapter 4 provides a description of the design process of 3 different flow calming structures and their construction. In Chapter 5 results of the tests and comparison between tested flow calming structures are provided. Potential application and limitations of this work are discussed in Chapter 6. At last, Chapter 7 presents the conclusion of the research and suggestions for future research.

2 Literature review

A brief literature review was performed to address challenges within the design of flow calming structures and their use in sand traps. When looking for information, it has been found that there is no clear vocabulary related to flow calming structures. One can find the same or similar element with different names, for instance, flow calming structures, tranquilizer racks, streamline rectifiers or honeycombs. The structures founded during literature study were mainly for use in experimental flumes where they are installed to break up poor velocity profiles and develop uniform flow parallel to the longitudinal axis of the flume. They are usually installed in groups of two or three, where the first rack breaks up the poorly conditioned flow and the remaining racks form the flow before it enters the point of measurement. Use of tranquilizer racks in flumes is required when there is not sufficient straight run of pipes upstream of the flume, and therefore uniform flow cannot develop on its own (Open channel flow; Tracom fiberglass products).

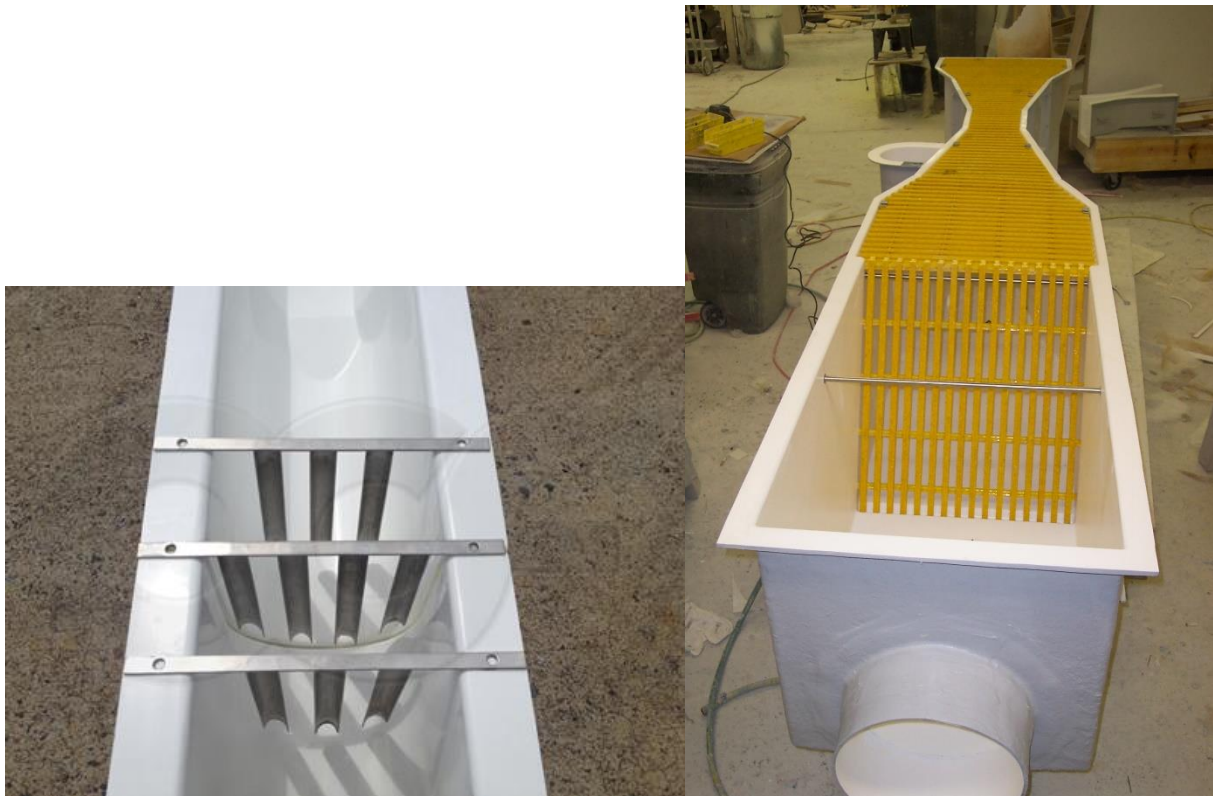


Figure 1 Tranquilizing rack for use in an experimental flume (Open channel flow; Tracom fiberglass products).

The only flow calming structure not used in an experimental flume was found in a research article written by Paschmann (2017). Here the author presented a picture taken in a sand trap of one HPP in Switzerland (Figure 2).

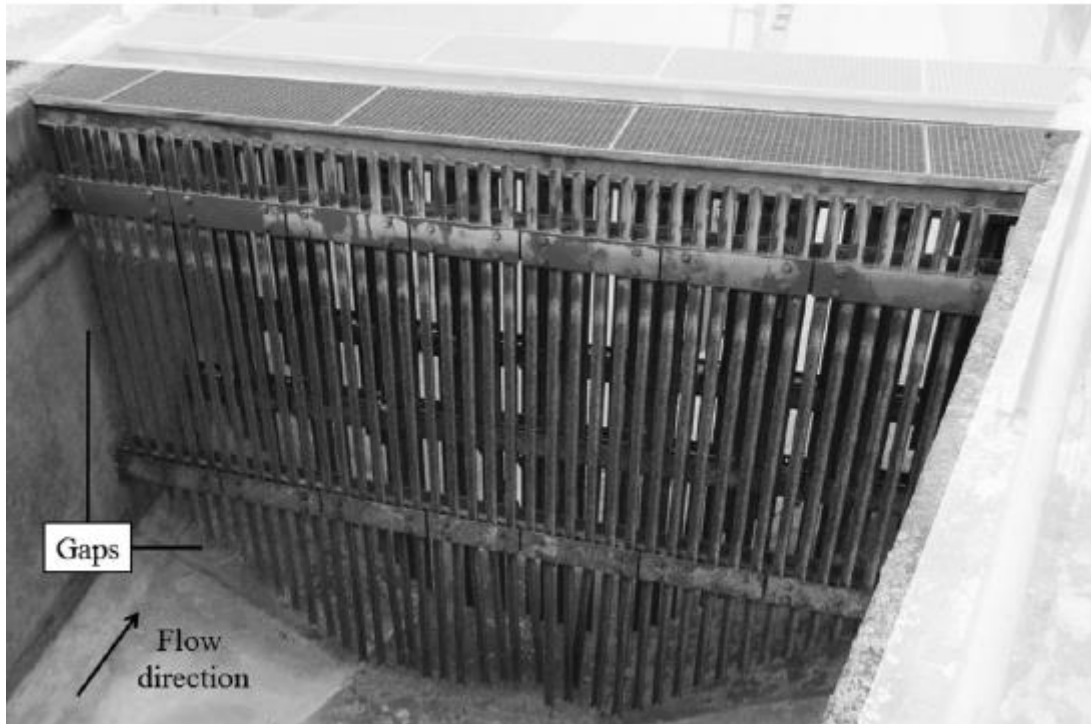


Figure 2 Three rows of tranquilizing racks (Paschmann et al., 2017)

However, there was no information about the design of such a structure included. On the other hand, the article provided contact information to the author. From email conversation between Ola Haugen Havrevoll and Christopher Paschmann was clear that most of HPP in Switzerland are equipped with tranquilizing racks in sand traps to calm and homogenize the entering flow. Unfortunately, even he did not have information about why this design is so common and on what is it based.

The literature review has revealed a gap in research focused on design and use of flow calming structures and did not provide enough information for the design of three different flow calming structure. An explanation of what the design of the structures is based on is provided in Chapter 4.4.

3 Theory

3.1 General hydraulics

3.1.1 Continuity equation

The principle of conservation of mass is applied for flowing fluid where the mass of fluid in the control volume remains constant for steady flow. From here the equation (1) of continuity for the flow of a compressible fluid through a streamtube with the mean velocity in the profile is equal:

$$\rho_1 A_1 \bar{u}_1 = \rho_2 A_2 \bar{u}_2 = \text{constant}, \quad (1)$$

where ρ_1 and ρ_2 are densities [kg/m^3] and u_1 and u_2 are mean velocities [m/s] measured at the profiles with the cross-sectional areas A_1 and A_2 [m^2]. Assuming the incompressible fluid, so that $\rho_1 = \rho_2$, expressed as the mass rate of flow equation (1) can be reduced to:

$$A_1 \bar{u}_1 = A_2 \bar{u}_2 = Q, \quad (2)$$

3.1.2 Bernoulli's principle

Change of momentum from profile to profile along with a streamline together with the forces acting due to the surrounding pressure and changes of elevation is given by relationship between velocity, pressure, elevation, and density along a streamline. Bernoulli defined the relationship (3) between pressure energy, kinetic energy and potential energy as energy per unit weight assuming steady flow with a frictionless fluid of constant density:

$$z + \frac{P}{\rho g} + \frac{v^2}{2g} = \text{constant}, \quad (3)$$

where z is elevation [m], P is pressure [Pa], ρ is density [kg/m^3], g is gravitational acceleration [m/s^2] and v is mean velocity [m/s]. However, for the purposes in open channels (i.e., laboratory flume) of closed conduits, Bernoulli's equation must be supplied for energy which has been lost between two profiles due to work against friction or in a machine such as a turbine. Thus, the total energy per unit weight at profile 1 is equal to total energy per unit weight at profile 2 and loss per unit weight (4):

$$z_1 + \frac{P_1}{\rho g} + \frac{v_1^2}{2g} = z_2 + \frac{P_2}{\rho g} + \frac{v_2^2}{2g} + h, \quad (4)$$

where z_1 is elevation from reference at profile 1 [m], P_1 is pressure at profile 1 [Pa], ρ is density [kg/m³], g is gravitational acceleration [m/s²] and v_1 is mean velocity at profile 1 [m/s], z_2 is elevation from reference at profile 2 [m], P_2 is pressure at profile 2 [Pa], ρ is density [kg/m³], g is gravitational acceleration [m/s²] and v_2 is mean velocity at profile 2 [m/s] a h is loss [m].

3.1.3 Energy losses

Aspects to be considered during the design of hydropower systems are hydraulic principles, together with optimization of tunnel alignment, size, shape, followed by the detailed design of intakes, transition, sand traps, gate plugs, and other related structures (Lysne, Glover, Støle, & Tesaker, 2003). Each of the mentioned structures has an essential role in the design process as they affect the head loss due to friction, bends, transition and others. The total hydraulic loss is dominated by friction losses, and therefore should be minimized. The friction losses (5) can be determined using the Darcy-Weisbach friction equation:

$$h_f = f \frac{L \cdot v^2}{D \cdot 2g}, \quad (5)$$

where h_f is head loss [m], f is dimensionless coefficient [-], L is length [m], v is mean velocity [m/s], D is diameter [m], g is gravitational acceleration [m/s²]. Determination of the Darcy friction factor is related to the effect of viscosity ν and depends on the flow conditions, which can be estimated by the Reynolds number Re (6). Moody diagram including all types of flow (laminar, critical, transition and fully developed turbulent flow) is practical and sufficient for identifying a suitable value for f . However, it ought to be mentioned that many hydropower design applications occur under fully developed turbulent conditions.

$$Re = \frac{D \cdot v}{\nu}, \quad (6)$$

where D is conduit diameter [m] (can be substituted with R (hydraulic radius) [m] for open channel flows), v is mean velocity [m/s] and ν is kinematic viscosity of the fluid [m²/s]. The Reynolds number for laminar flow is lower than 1000 for closed conduits (lower than 500 for open channels), for critical and transition flow between 2300-4000

for closed conduits (between 500-2000 for open channels) and for fully developed turbulent flow larger than 4000 for closed conduits (larger than 2000 for open channels).

Another type of losses (with negligible effect) called singular losses is related to structures which create an obstruction in the flow or which changes the flow direction (7).

$$h_s = s \frac{v^2}{2g}, \quad (7)$$

where h_s is head loss [m], s is dimensionless singular coefficient [-], v is mean velocity [m/s] and g is gravitational acceleration [m/s²].

3.2 Erosion, sediment transport, and deposition

Erosion, mass transport, and deposition are natural processes in watercourses and tunnels with sediments. These processes are shown in Figure 3.

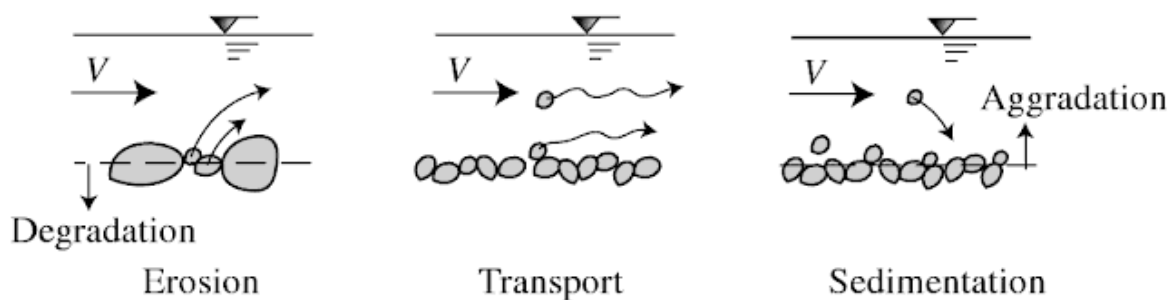


Figure 3 Processes of erosion, mass transport and sedimentation (Julien, 2010)

3.2.1 Erosion

Erosion is the physical process of disrupting and removing part of the Earth's surface by external factors such as wind and water. The water applies destabilising forces on a particle often referred to as drag and lift. When these forces are strong enough to initiate motion, particles begin to slide, roll and saltate down the river bed. While the drag works in the main direction of the flow and has to exceed the frictional and gravitational forces, the lift works transversally to the flow direction and comes from pressure differences caused by velocity variation over the particle.

$$F_D = C_D \cdot A \cdot \rho \cdot \frac{v^2}{2}, \quad (8)$$

$$F_L = C_L \cdot A \cdot \rho \cdot \frac{v^2}{2}, \quad (9)$$

where F_D is drag force [N], F_L is lift force [N], C_D is the drag coefficient [-], C_L is lift coefficient [-], A is the area of exposure to the flow [m²], ρ is the density of water [kg/m³], and v is the water velocity [m/s] (Lysne et al., 2003).

When examining areas with erosion problems, one should look into three parameters. Firstly, the water velocity close to the bed where erosion happens. Unfortunately, this one is difficult to measure and therefore not often used. Secondly, the average velocity in the flow which comes from the velocity distribution depending on the cross-section, depth, and roughness. This parameter is easier to get, but at the same time, it may not give correct results. Lastly, the shear stress along the bed related to fluid viscosity. An average value of shear stress is easy to calculate and gives a good estimation of the shear stress. Critical shear stress, also called critical Shields parameter is the stress at which motion of the sediments occurs. For calculation of critical shear stress, drag and lift as the destabilizing forces and weight and friction as the stabilising forces act against each other.

In uniform flow, the bed shear stress is found as

$$\tau_0 = g \cdot \rho_w \cdot R \cdot I, \quad (10)$$

where τ_0 is bed shear stress [N/m²], ρ_w is the density of water [kg/m³], R is hydraulic radius [m], and I is the slope of energy line [-].

Knowing the bed shear stress, critical Shields stress can be calculated as

$$C_s = \frac{\tau_0}{(\rho_s - \rho_w)gd_s}, \quad (11)$$

where C_s is critical Shields stress, τ_0 is bed shear stress [N/m²], ρ_s is the density of sediments [kg/m³], ρ_w is the density of water [kg/m³], g is gravitational acceleration [m/s²], and d_s is the diameter of sediment [m].

Critical Shields stress is represented in Shields' diagram (Figure 4) by the Shields' curve, which is a function of the boundary Reynolds number Re^* .

$$Re^* = \frac{u^* d_s}{\nu}, \quad (12)$$

$$u^* = \sqrt{gRI} = \sqrt{\frac{\tau_0}{\rho}}, \quad (13)$$

where Re^* is boundary Reynolds number [-], u^* is shear velocity [m/s], d_s is diameter of sediments [m] and ν is kinematic viscosity of water [m²/s].

With the critical Shields parameter and the boundary Reynolds number, one can get Shield diagram showing the border between no sediment motion (under Shields curve) and sediment motion (over Shields curve) (Lysne et al., 2003; Shields, 1936).

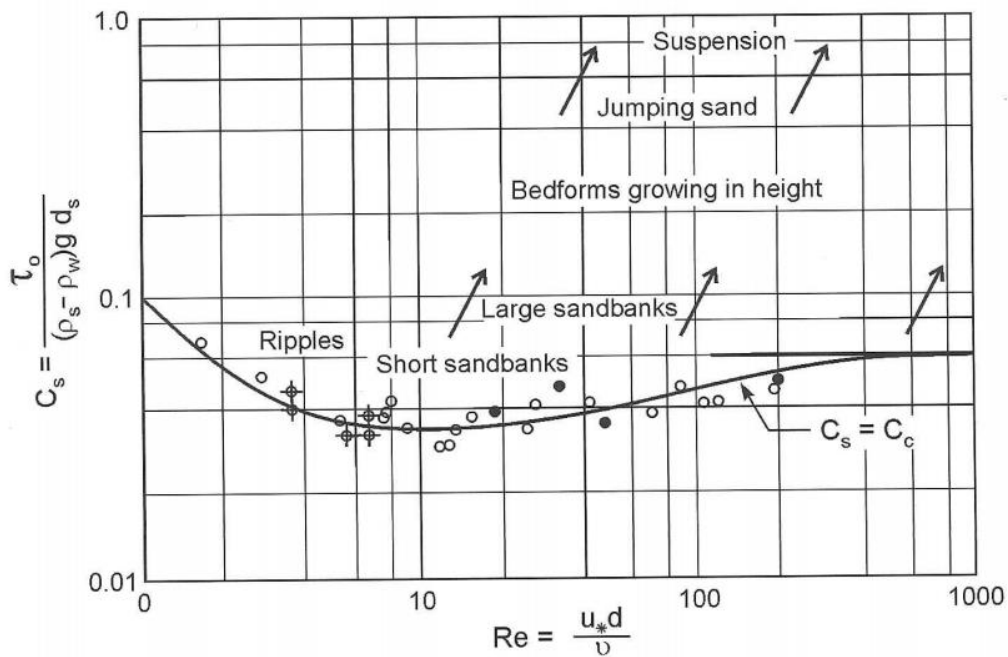


Figure 4 Shields' diagram for start of motion (Lysne et al., 2003)

3.2.2 Mass transport

Mass transport occurs when the bed shear stress exceeds the critical bed shear stress, and particles are set in motion. Mass transport is often divided into three types- bed-load transport, suspended-load transport, and wash-load transport. All of these are shown in Figure 5.

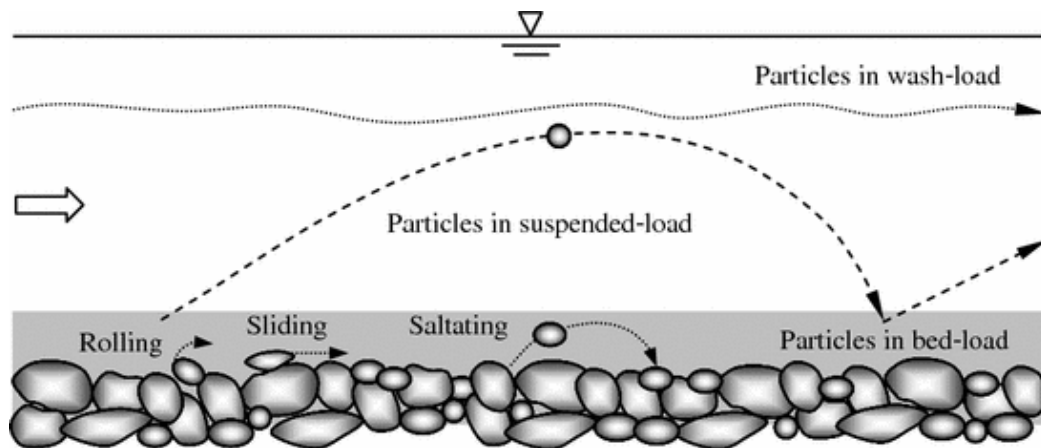


Figure 5 Different modes of sediment transport (Dey, 2014)

In the bed-load transport particles are rolling, sliding and saltating, while in suspended load particles are kept in suspension in the water (Dey, 2014). The boundary between bed-load and suspended-load is not clear. However one can say that when the shear velocity is higher than the settling velocity of the particle, the particles are suspended.

3.2.3 Deposition

The sediment will deposit when the ability of water to transport particles decreases due to a decrease in discharge, decrease in water velocity or a combination of both. The decrease in discharge and water velocity occurs mainly due to changes in geometry for instance decrease of a slope or change of a cross-section area, and first affects the bigger particles. This leads to a natural sorting of sediments meaning that the biggest particles settle first while the finer particles are transported further.

3.3 Dimensional analysis and similitude

Dimensional analysis is a mathematical technique used for analysing of the relationship between different physical quantities. With a combination of five fundamental dimensions, most of the physical quantities can be expressed. These fundamental dimensions are time, mass, length, temperature, and electrical current, and they have their respective units which are chosen, for instance, miles vs. kilometres, or pounds vs. kilograms. They can be easily measured in experiments. The basic principle of dimensional analysis is dimensional homogeneity, meaning that on both sides of equation dimensions of each term are equal. If the number of variables involved in the linear equation is known, the relationship among the variables can be determined by **Buckingham's π -Theorem**. If there are n variables with m fundamental dimensions, the

variables are arranged into $(n-m)$ dimensionless parameters, called π -terms (Douglas J. F., 2011).

Similitude is a concept used in the testing of engineering models. A model has similitude with the prototype if they share geometric, kinematic and dynamic similarity.

Geometric similarity is the similarity of shape. It is achieved when the ratios of corresponding linear dimensions are equal.

$$L_r = \frac{L_m}{L_p}, \quad (14)$$

where L_r is length scale ratio [-], L_m is the length of the model [m], and L_p is the length of the prototype [m].

Kinematic similarity is the similarity of motion. It is achieved when the ratio of forces at corresponding points are equal.

$$v_r = \frac{v_m}{v_p} = \frac{v_{m1}}{v_{p1}} = \frac{v_{m1}}{v_{p1}}, \quad (15)$$

$$a_r = \frac{a_m}{a_p} = \frac{a_{m1}}{a_{p1}} = \frac{a_{m1}}{a_{p1}}, \quad (16)$$

where v_r is velocity scale ratio [-], v_m is the velocity in the model [m/s], v_p is the velocity in the prototype [m/s], a_r is acceleration scale ratio [-], a_m is the acceleration in the model [m/s²], a_p is the acceleration in the prototype [m/s²].

Dynamic similarity is the similarity of forces. It is achieved when the ratio of velocity and acceleration at corresponding points are equal.

$$F_r = \frac{F_m}{F_p}, \quad (17)$$

where F_r is force scale ratio [-], F_m is the force in the model [N], and F_p is the force in the prototype [N] (Buckingham, 1914; Ettema, Arndt, Roberts, & Wahl, 2000).

3.4 Hydraulic scale modelling

Scaling of the prototype has to follow scaling laws to get the right results. It is necessary to neglect less important parameters in order to simulate the more important ones. The two most commonly used scaling laws are Reynolds' and Froude's scaling law.

3.4.1 Reynolds' scaling law

Reynolds' scaling law is used when viscous forces are dominant what is mainly in pressurized flow. It is obtained by equating the model and the prototype versions of Reynolds' number. Reynolds' number is a ratio between kinetic forces and viscous forces.

$$Re = \frac{F_i}{F_v} = \frac{\rho v^2 L^2}{\mu v L} = \frac{\rho v L}{\mu} = \frac{v L}{\nu}, \quad (18)$$

where Re is Reynolds' number, F_i are kinetic forces [N], F_v are viscous forces [N], ρ is density of water [kg/m^3], v is water velocity [m/s], L is length, μ is dynamic viscosity and ν is kinematic viscosity [m^2/s].

By using Reynolds' scaling law, followed scales ratios can be expressed:

$$\text{Length} \quad L_r = \frac{L_m}{L_p}, \quad (19)$$

$$\text{Velocity} \quad v_r = \frac{v_r}{L_r} = \frac{1}{L_r}, \quad (20)$$

$$\text{Time} \quad t_r = \frac{t_m}{t_p} = \frac{L_m v_p}{v_m L_p} = \frac{L_r}{v_r} = L_r^2, \quad (21)$$

$$\text{Discharge} \quad Q_r = v_r A_r = \frac{v_m A_m}{v_p A_p} = \frac{1}{L_r} L_r^2 = L_r. \quad (22)$$

3.4.2 Froude's scaling law

Froude's scaling law is used when gravitational forces are dominant what can, for instance, be sediments depositing in sand traps or open channel with free surface flow. However, it can also be used for scaling of parameters for pressurized flow. It is obtained by equating the model and the prototype versions of Reynolds' number. Froude number is a ratio between kinetic forces and gravitational forces.

$$Fr = \frac{F_i}{F_g} = \frac{\rho v^2 L^2}{\rho g L^3} = \frac{v^2}{gL} = \frac{v}{\sqrt{gL}}, \quad (23)$$

where Fr is Froude's number, F_i are kinetic forces [N], F_g is gravitational forces [N], ρ is density of water [kg/m^3], v is water velocity [m/s], L is length and g is gravitational acceleration [m/s^2].

By using Froude's scaling law, followed scales ratios can be expressed:

Length
$$L_r = \frac{L_m}{L_p}, \quad (24)$$

Velocity
$$v_r = \sqrt{L_r}, \quad (25)$$

Time
$$t_r = \frac{t_m}{t_p} = \frac{L_m v_p}{v_m L_p} = \frac{L_r}{v_r} = \frac{L_r}{\sqrt{L_r}} = \sqrt{L_r}, \quad (26)$$

Discharge
$$Q_r = v_r A_r = \frac{v_m A_m}{v_p A_p} = \sqrt{L_r} L_r^2 = L_r^{2.5} \quad (27)$$

4 Research methods

4.1 Description of the prototype

Tonstad hydropower plant is located in Sirdal municipality in Vest-Agder county. Five Francis turbines with a total installed capacity of 960 MW are in use. The first two units of 160 MW each started to operate in 1968. In 1971, two units of the same size were added. The fifth unit of 320 MW is in operation since 1988. Based on the annual production of 3800 GWh, Tonstad hydropower plant is the largest power plant in Norway. The gross head of Tonstad hydropower plant is 450 metres. Power plant intake is located in the lake Homstølvatnet and water is discharged through the power plant into the lake Sirdalsvatnet (Sira-Kvina Kraftselskap). Originally, Tonstad HPP was designed with two sand traps that were modelled in River and Harbour Research Laboratory at the Technical University of Norway (NTH). Sand trap 3, the third sand trap, was put into operation in 1988 without being modelled in a laboratory (NTH, 1967). Figure 6 shows the system of three sand traps of Tonstad HPP. The geometry of sand traps 1 and two was drawn based on Sira-Kvina power company's drawings presented in Appendix A. For sand trap 3, 3D scanning of the sand trap was done (Brevik, 2013).

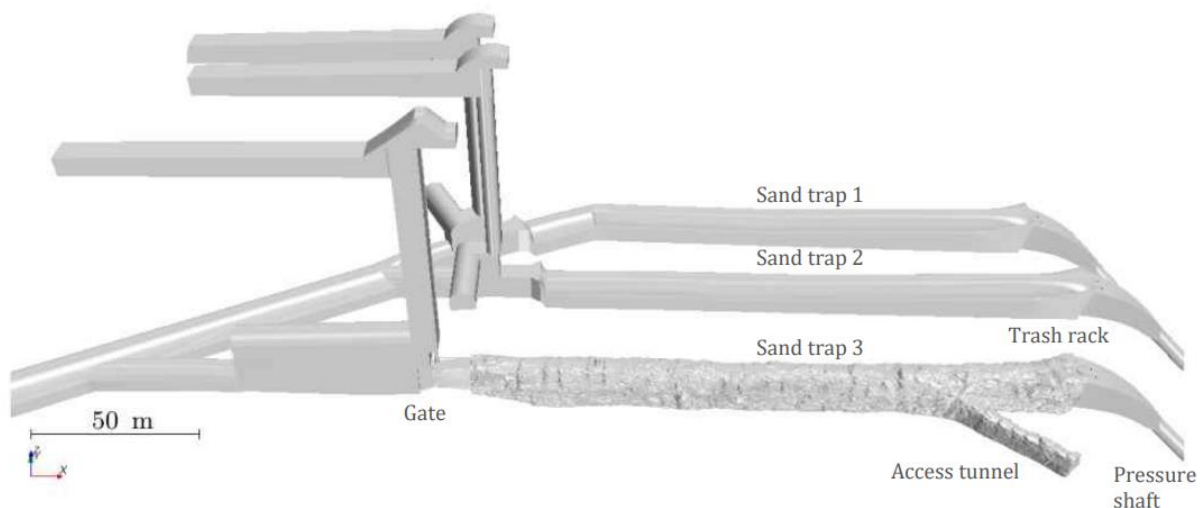


Figure 6 System of sand traps of Tonstad HPP (modified after Brevik, 2013)

As mentioned before, the prototype has experienced operational problems that have resulted in sand and gravel transport into penstock and subsequent turbine damage. The origin of these problems might be a sliding gate in the upstream end of the sand trap. The gate is 4 m wide and 7 m high giving a cross-sectional area of 28 m² while the cross-

sectional area of the sand trap is 119 m^2 . Assuming constant flow, based on the continuity equation, water velocity increases when passing through the gate, and therefore sediments are not trapped adequately. When the sand trap is filling with water after being shut, the gate is lifted 4 cm, and maximum discharge is estimated to be $4.5 \text{ m}^3/\text{s}$ with a maximum velocity of 28 m/s respectively (Sira-Kvina Kraftselskap, 2016).

Downstream of the gate there is 16 m long horizontal section of the tunnel with a cross-sectional area of 70 m^2 ($W \times H = 7 \times 10 \text{ m}$) followed by a diffuser with a gradually increasing cross-sectional area from 70 to 119 m^2 , changing its shape from rectangular to the cross-section shown in Figure 7, and a slope of 1:6 on a length of 16 m.

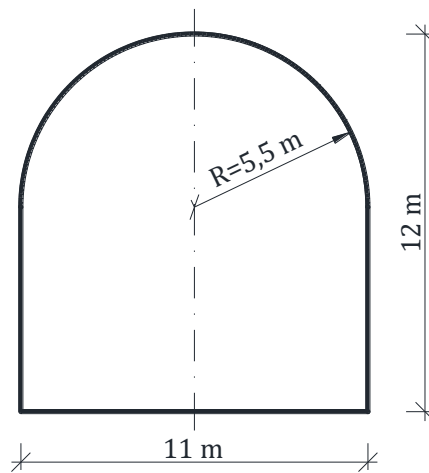


Figure 7 Cross-section of the sand trap

When continuing downstream, the sand trap itself is following. The upper 79 m of the sand trap is in slope 1:23.8, while the lower 80 m of the sand trap, upstream of the trash rack, is level. An access tunnel to the sand trap is connecting 40 m upstream of the trash rack (measured to the central axis of the access tunnel). During operation of the HPP, the access tunnel is closed by a concrete plug. The turbine regulates the flow in a range between 40 and $80 \text{ m}^3/\text{s}$ which gives an average velocity of 0.67 m/s in the sand trap (Sira-Kvina Kraftselskap, 2016).

4.2 Description of the hydraulic scale model

The hydraulic laboratory at NTNU was entrusted to build the physical hydraulic scale model of Tonstad HPP's sand trap 3. The physical model was scaled using Froude scaling law, as gravity and inertia were the dominant forces. The model was also influenced by viscous forces controlling turbulences, but these were scaled correctly in view of the turbulent regime ($Re > 3000$) in the prototype and the model. Water elasticity was neglected, considering water as incompressible. The geometrical scale of the model was 1:20. For the construction of the model, plexiglass with a thickness of 12 mm was used, and the sand trap was built with a double bottom allowing vertical expansion of the sand trap. Pressure shaft and outlet pipe, as the lowest points of the model, and an inflow basin securing pressurized flow, as the highest point, affected the vertical layout of the model. Drawings of the physical model done by engineer Geir Tesaker and modified by the author of this thesis are presented in Figure 8 and Figure 9.

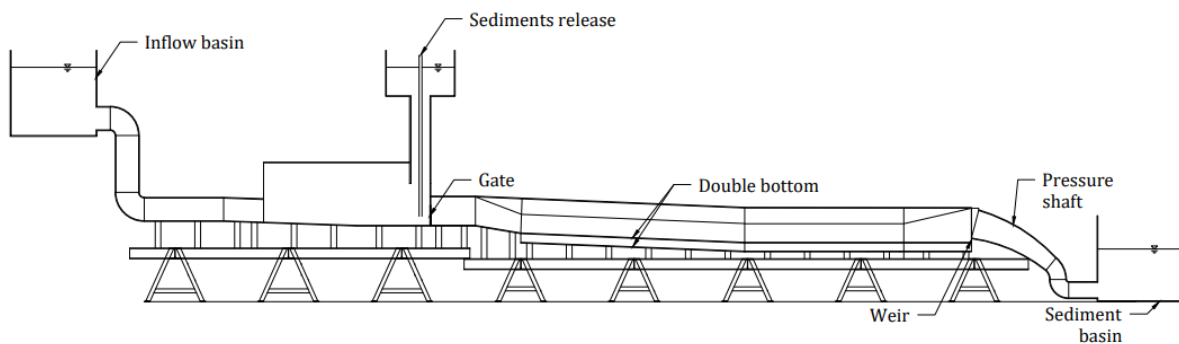


Figure 8 Drawing of the hydraulic scale model of Tonstad HPP

Unfortunately, the model was due to several unpredictable complications causing delays still under construction at the time when the experiments needed to be done. Therefore, it was decided to use another alternative, an already existing model which is described in Chapter 4.3. Even though the model of the sand trap was not used, information about instrumentation and measurements to be done are provided in Chapter 4.2.1.

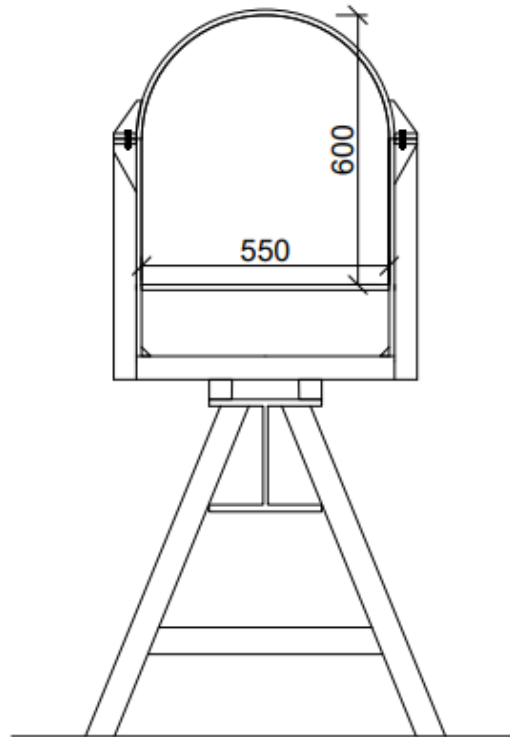


Figure 9 Cross-section of sandtrap model

4.2.1 Instrumentation and measurements

To secure a stable water pressure in the model, a weir is installed in the inflow basin accompanied by ultrasonic measurement of water level. Water inflow to the model and outflow from the model are measured by magnetic inductive discharge metres (MID) to control the discharge in the model. Head loss over the system is measured by differential pressure gauges installed in the surge tank and outlet pipe. Sediments are supplied to the model from the surge tank just upstream of the gate to secure that all sediments will enter the sand trap. In case of some sediments passing through the sand trap, a sediment basin is built downstream of the pressure shaft to collect them. In addition, a filter is located on the outlet pipe from the sediment basin, to capture the rest of the sediments. Deposition of the sediments is recorded by top-mounted and side-mounted cameras.

4.3 Description of the experimental flume used for experiments

As mentioned before, it was not possible to use the model of the sand trap for the experiments. Therefore, an already existing dimensionally similar experimental flume was used. Even though the models are dimensionally similar, there was a major difference in a type of flow. While in the prototype and sand trap model flow was pressurized, the

experimental flume was an open channel. Since the idea of the experiments was to compare three different flow calming structures based on their headloss, impact on the trapping efficiency of the sand trap and sediments distribution in the sand trap, the experimental flume was considered as a good alternative to the unfinished sand trap model.

The experimental flume was made as a closed system with recirculation. It had a rectangular cross-section, 0.75 m high and 0.6 m wide giving a difference of 5 cm of the width in comparison with the original sand trap model. To have the same cross-sectional area as the original sand trap model, the flume had to be filled to a height of 0.5 m. The total length of the flume was approximately 30 m where 17.5 m are suitable for installation of model components allowing replicating the original sand trap model. Figure 10 presents the experimental flume and its layout used for the experiments.

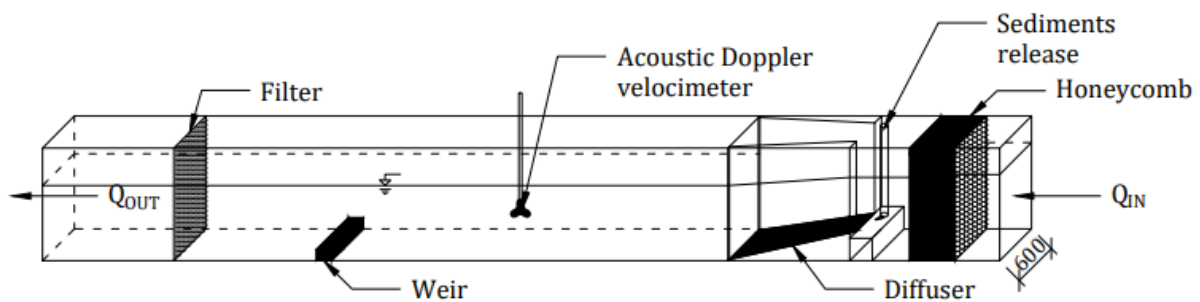


Figure 10 Setup of the experimental flume

The model was equipped with a honeycomb installed most upstream in the model ensuring stable inflow conditions (Figure 11) followed by a structure representing the diffuser. Over the diffuser, a vibrating dosing machine was placed to have the sediments released into the model in the place with the highest possible velocity (Figure 12).



Figure 11 Honeycomb installed most upstream in the flume ensuring stable inflow conditions

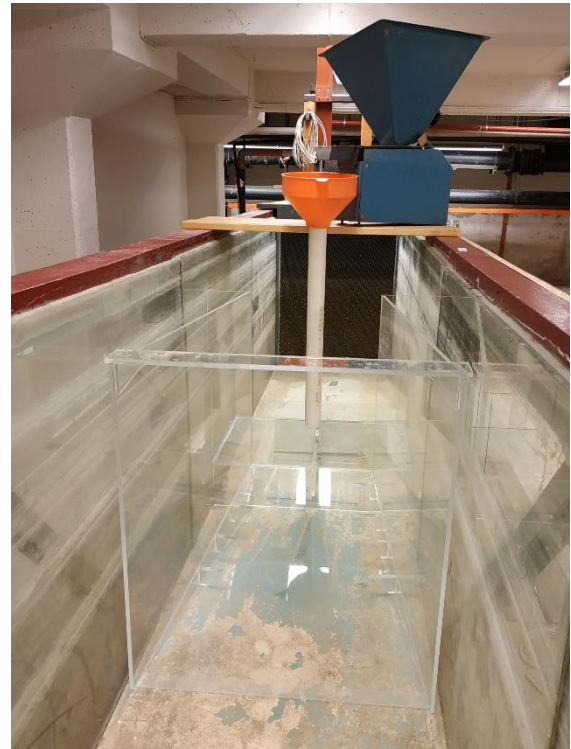


Figure 12 Provisional diffuser with a vibrating dosing machine

8 m downstream from the diffuser, a 7.5 cm high weir was installed creating the end of the sand trap in the flume (Figure 13).



Figure 13 Weir creating the end of the sand trap (view from the upstream on the left side, side view on the right side)

Downstream of this weir, there was a 5 m long part of the flume where sediments not trapped in the sand trap could deposit. At the most downstream end of the flume, a filter was placed to secure that no sediments would be drawn into the circulation system.



Figure 14 Filter placed most downstream in the flume

The maximum discharge in the prototype is $80 \text{ m}^3/\text{s}$. With a scaling factor for discharge $Q_r=L_r^{5/2}=1:1789$, an equivalent discharge in the model was 45 l/s . An equivalent discharge for filling of the sand trap was 2.5 l/s in the model, while $4.5 \text{ m}^3/\text{s}$ in the prototype. For the time, the scaling factor was $T_r=L_r^{1/2}=1:4.47$, meaning that the deposition that occurred in the prototype during one year would take 82 days in the model. When considered that at least eight experiments had to be done, scaling of time could not be done based on Froude law. Steinkjer (2018) used another approach in her thesis, where the author considered that the equivalent amount of sediments for one year in the prototype would be inserted to the model evenly for 90 minutes.

Similarly, for filling and emptying of the sand trap, another approach was chosen. Filling of the sand trap takes 1.5 hours in the prototype, equal to 20 minutes in the model, and emptying of the sand trap takes 75 hours in the prototype, meaning 17 hours in the model. Both procedures were done in about one hour each(Steinkjer, 2018).

Sediments used for the experiments were chosen based on the research done by Steinkjer (2018). In the research, three different types of sediments were modelled, including sand, carbonate rock and a lightweight material- poly-methyl methacrylate (PMMA). Every material had its positive and negative sides. However, PMMA was proposed to represent

particles with sizes 1.4 – 4.1 mm in the prototype, and sand to represent particles with sizes 2.5 – 10.0 mm in the prototype (Steinkjer, 2018). However, considering research done in the present thesis, where flow calming structures were installed in the model to achieve calming of the flow and increase sand trap efficiency, it was not possible to use PMMA because of its particle size, which might cause clogging of the flow calming structures. Therefore, the sand used and proposed by Steinkjer (2018) was used as a material representing sediments also in all the experiments done in this research. This sand has a density of 1600 kg/m^3 and a particle size between 0–0.5 mm. The particle size distribution of the sand is presented in Figure 15.

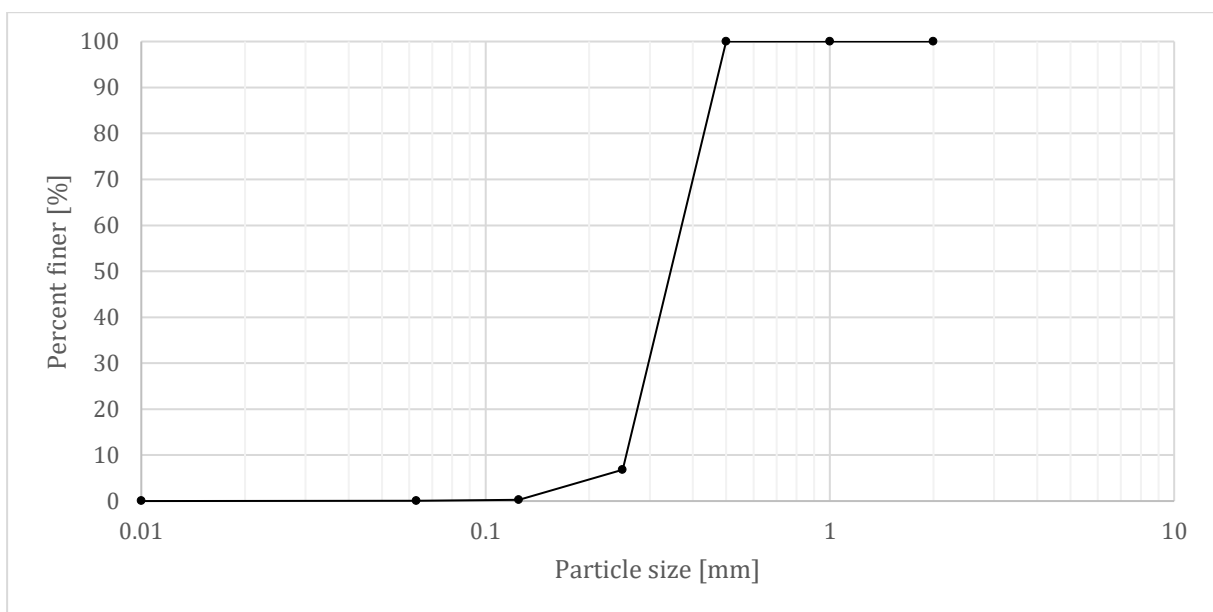


Figure 15 Particle size distribution of the sand used in the experiments

The sediment load cumulated in the prototype presents $60 \text{ m}^3/\text{year}$, giving a sediment load of 7.5 l in the model. However, due to the inaccuracy of volume measurement, the sediment load was measured by weight, when for sand with a density of 1600 kg/m^3 , 7.5 l is equal to 12 kg.

4.3.1 Instrumentation and measurements

In the experimental flume, an acoustic Doppler velocimeter (ADV) was installed giving information about flow velocity continuously every second (Figure 16). Knowing the velocity of the flow and cross-sectional area, the discharge can be calculated. The sediment accumulation in the sand trap was documented by taking photos. For one of the experiments, a time-lapse video was made to show the accumulation of the sediments over time. Sand trap efficiency was calculated as a ratio of the mass of sediments trapped in the sand trap and the mass of inserted sediments. For this purpose, sediments had to be free of moisture. Sediments were drying in an oven at a temperature of 105 °C until the sediments mass has equilibrated. Headloss in the sand trap was measured as a difference in water depth upstream of the diffuser and on the very end of the sand trap.



Figure 16 Acoustic Doppler velocimeter installed in the flume

4.3.2 Running of the experiments

For every experiment, the same conditions had to be secured. The flume was emptied and cleaned and afterwards filled with water up to 0.5 m. The process of filling the flume took approximately 45 min. After the flume was filled to the required height, the pump in the recirculation was turned on and was running 15 minutes to provide stable conditions for the experiment. The experiment started with turning the vibrating dosing machine on and releasing of the sediments into the model over 90 minutes. During the experiment, water

depths were measured to provide information about headloss. When all the sediments were released, the test run for another 5 minutes to allow the sediments released as the last to deposit. Then the pump was turned off, pictures of the deposition of the sediments were taken, and water was slowly drained out within one hour. After emptying, the sediments were collected separately from the sand trap, and the flume downstream of the weir, dried, weighted and sand trap efficiency was calculated. For the sediments collected downstream of the weir sieving analysis was done to see what was the size of the particles not caught in the sand trap.

4.4 Design of flow calming structures

In order to improve the performance of the current sand trap in Tonstad HPP, three different flow calming structures were designed to be tested in the hydraulic scale model of Tonstad HPP. The design was preceded by a literature study. However, the literature study provided information only about one structure. The other two flow calming structures were designed based on experiences and common practices used in the hydraulic laboratory for calming the entering flow to a flume.

4.4.1 Flow calming structure No. 1

The common practice of how to calm and homogenize flow entering a flume is using obstacles in the flow parallel with the flow. Such a structure is shown in Figure 17.

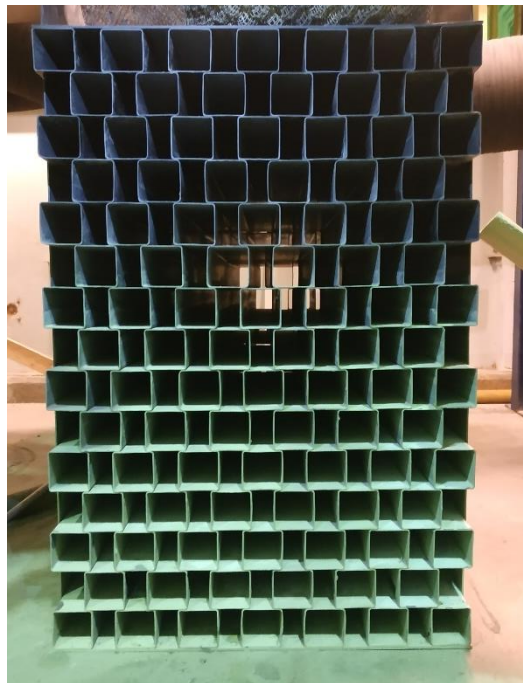


Figure 17 Flow calming structure used in hydraulic flumes

Since the flow calming structure was not installed in a prismatic flume but in a diffuser, the design had to be adjusted to secure even flow distribution. Therefore, expanding the structure along with the diffuser was necessary.

When considering building of this structure either in the model scale or in the prototype, one has to apply materials and methods that are available and simple to implement. In this case, the idea was to use concrete pipes with a diameter of 1000 mm in the prototype. When the model scaling factor 1:20 was applied, the diameter of 50 mm in the model was

obtained, and material with similar Manning's roughness coefficient was chosen. Concrete pipes have Manning's roughness coefficient $n=0.012$ and, therefore, as a material used for the model were chosen polyvinyl chloride pipes with $n=0.011$ (Chow, 1959). In total, 54 pipes with a length of 800 mm aligned in six rows were chosen. Design of this flow calming structure is presented in Figure 18, while the constructed model in Figure 19

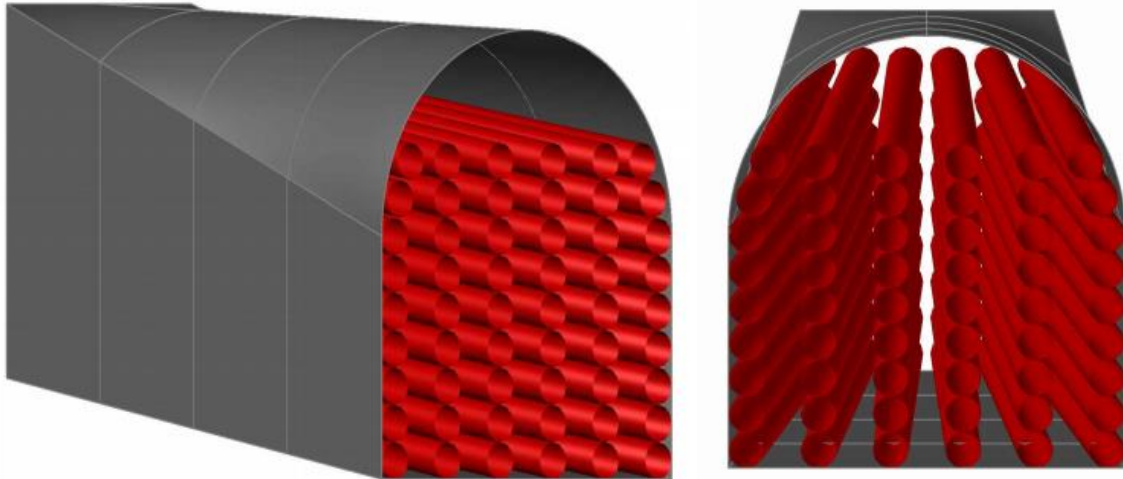


Figure 18 Design of flow calming structure No. 1



Figure 19 Photo of flow calming structure No. 1

4.4.2 Flow calming structure No. 2

In small models used for educational purposes, perforated plates are used to calm the flow. It can be used only one perforated plate or more as shown in Figure 20.

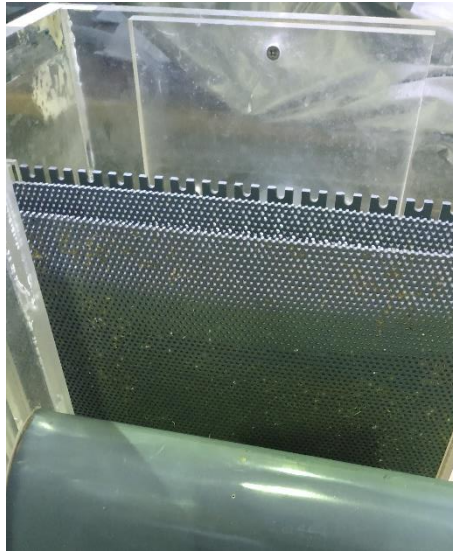


Figure 20 Flow calming structure used in small hydraulic models

Due to the lack of information about designing this kind of structure was found in the literature, the whole design was at the discretion of the author. In the prototype, this flow calming structure could be built as a concrete wall with circular openings with a diameter of 500 mm. As a material to be used for the model, 4 mm thick steel was chosen. Both, the concrete wall and the steel plate have Manning's roughness coefficient $n=0.012$. Design of perforated plate used as a flow calming structure is shown in Figure 21, and the model tested in the experimental flume is shown in Figure 22.

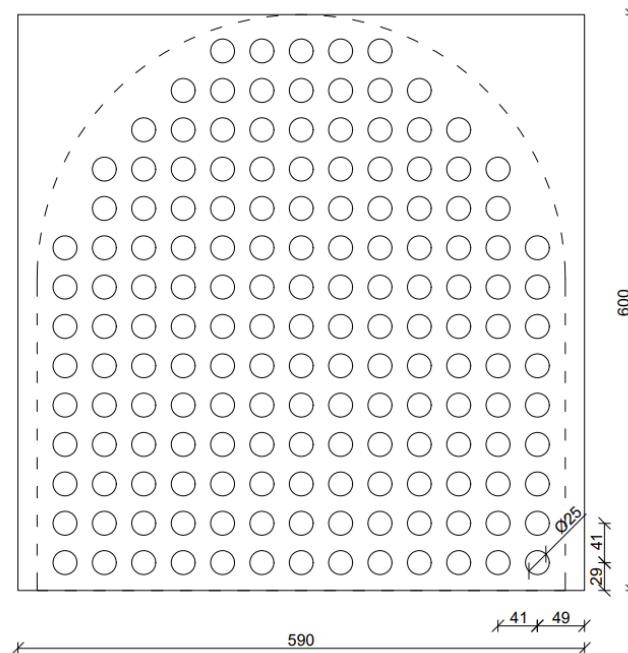


Figure 21 Design of flow calming structure No. 2, view from downstream

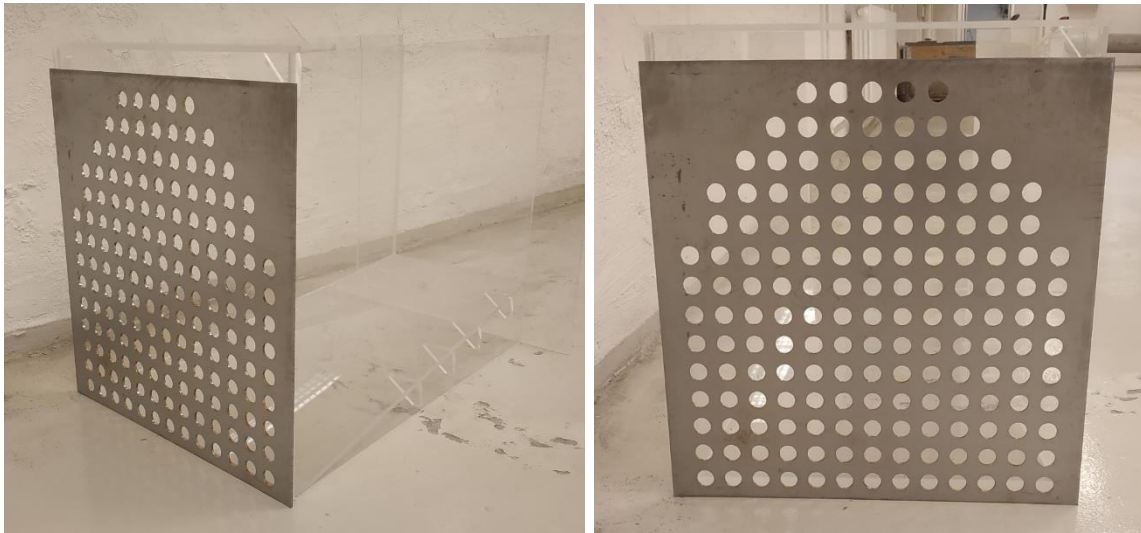


Figure 22 Photo of flow calming structure No. 2

4.4.3 Flow calming structure No. 3

Flow calming structure No. 3 was as the only one to which some information was found. Unfortunately, only a few pictures of this kind of structures (Figure 23) were available, without any additional information about distances between rows or individual rods. Therefore, all information about geometry had to be estimated from the pictures.

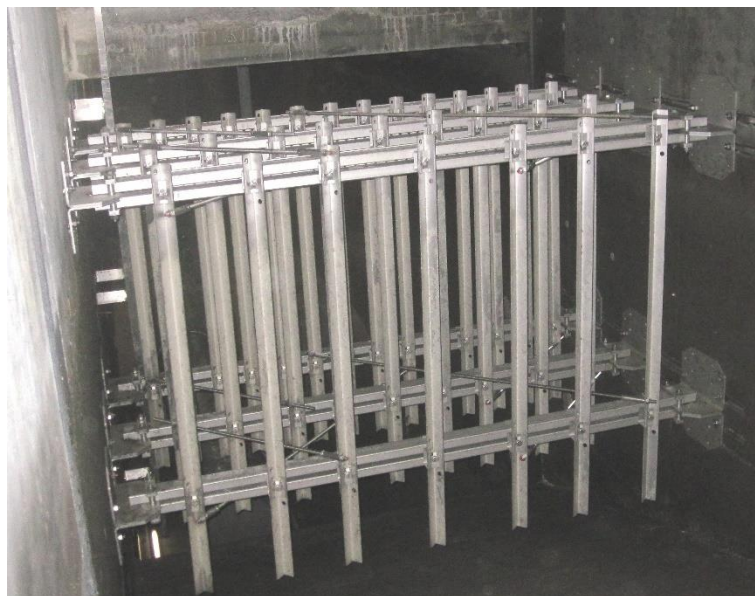


Figure 23 Flow calming structure used in a sand trap in Germany (SITEC)

Flow calming structure No. 3 was designed with four rows of vertical L-shaped rods with tips facing downstream. In the model were used 40 L-profiles with an arm length of 10×10 mm, meaning 200×200 mm in the prototype. It was made to be possible to test all four rows together, each one separately or any combination of two or three rows. This

design allows testing 18 different layouts from which three were tested in this research. Rows No. 1 and No. 3 (row No. 1 is the most upstream one, while row No. 4 is the most downstream one) were designed with a distance of 50 mm between the rods, while rows No. 2 and No. 4 had a distance of 40 mm between the rods. A number of rods in each row depends on the width of the diffuser in a certain location and on the designs distance between rods. Technical drawings of flow calming structure No. 3 showing all technical parameters are shown in Figure 24 and Figure 25.

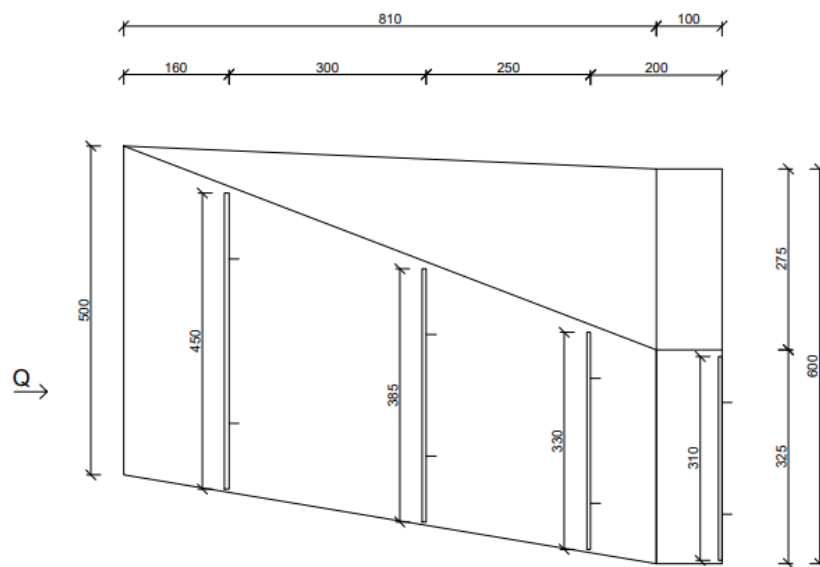


Figure 24 Design of flow calming structure No. 3, side view

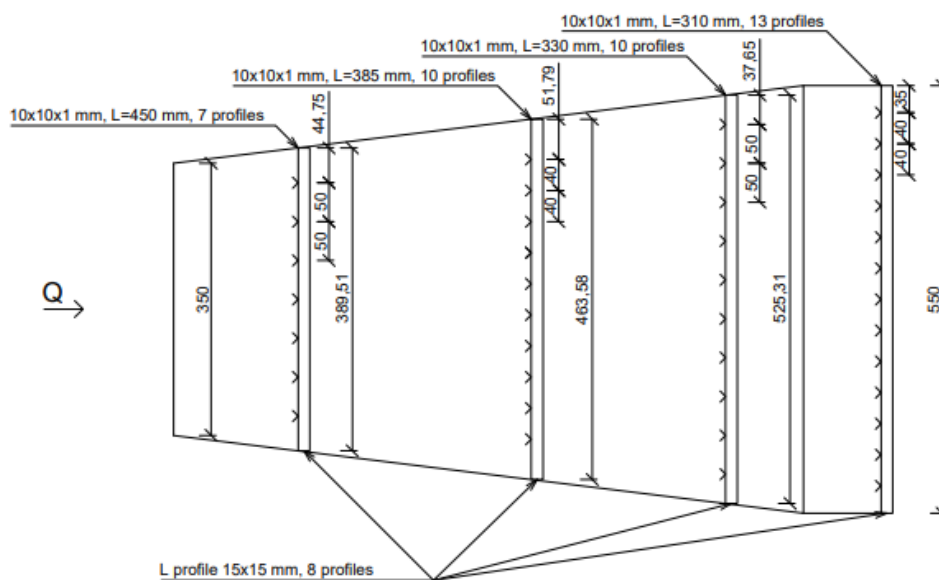


Figure 25 Design of flow calming structure No. 3, top view

4 Research methods

Figure 26, Figure 27 and Figure 28 show three layouts which were tested in the experimental flume.



Figure 26 Photo of flow calming structure No. 3, layout 1



Figure 27 Photo of flow calming structure No. 3, layout 2



Figure 28 Photo of flow calming structure No. 3, layout 3

5 Results

Nine tests were done in total: two without any flow calming structure, two tests with flow calming structure No. 1, two tests with flow calming structure No. 2, and three tests with flow calming structure No. 3, where three different layouts were tested. All the tests were done with maximum discharge equal to 45 l/s. An overview of the individual tests is given in Table 1.

Table 1 Overview of the tests done in the experimental flume

Type of test	Name of test	Discharge [l/s]	Velocity [cm/s]
No flow calming structure	Test 1	45	15
	Test 2	45	15
Flow calming structure No.1	Test 3	45	15
	Test 4	45	15
Flow calming structure No.2	Test 5	45	15
	Test 6	45	15
Flow calming structure No.3	Test 7	45	15
	Test 8	45	15
	Test 9	45	15

5.1.1 No flow calming structure

First two tests in the experimental flume were done without any flow calming structure in order to get an overview of the headloss in the system and behaviour of the sediments in the sand trap. In the tests, the sand trap efficiency of 95.83 % and 95.51 % was measured. Model tests results are presented in Figure 29. One could see that the sediments settled in both cases with the same pattern. The only difference is a mirror effect in the deposition. This might happen because the pipe bringing sediments to the model was not positioned precisely in the flume axis but tilted sideways. In the sand trap, ripple marks were formed due to the impact of current on the deposition of particles (Figure 30). Ripple marks are developed when the critical shear stress for the motion was exceeded by water flowing over the sediments (Bartholdy et al., 2015).



Figure 29 Results from test 1 (on the left side) and test 2 (on the right side) (view from upstream)

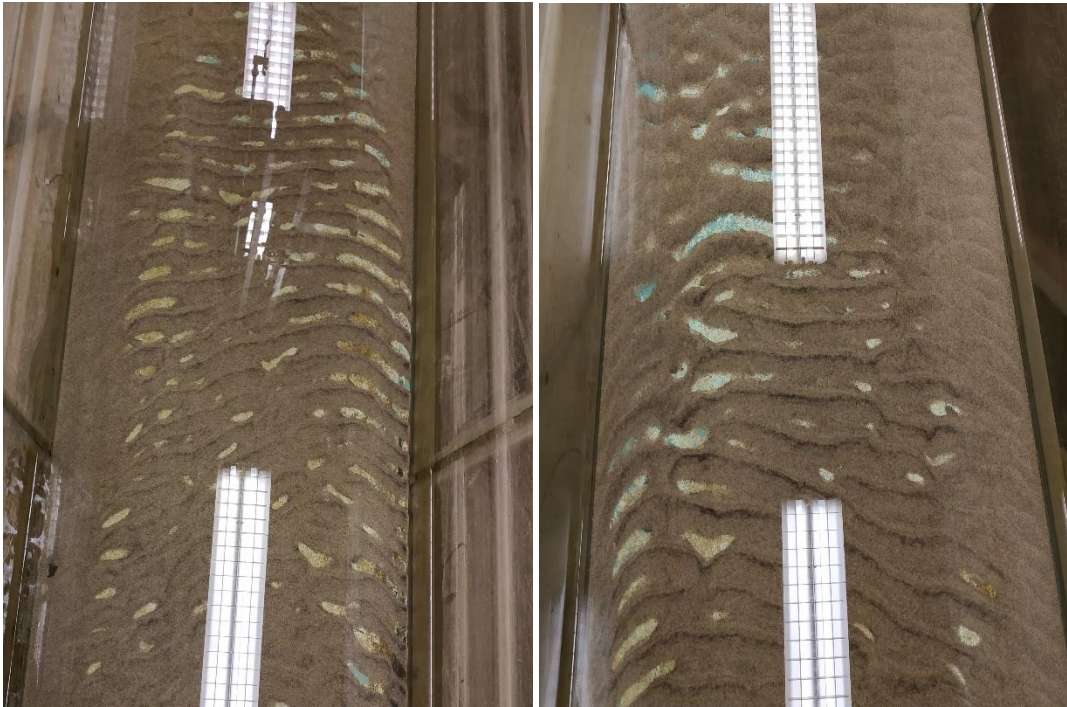


Figure 30 Detail of ripple marks developed during test 1 (on the left side) and test 2 (on the right side) (view from upstream)

Sediments collected from downstream of the sand trap were analysed after drying. 457 g of sediments were removed after the first test, and, alike, 489 g after the second test. As shown in results of sieve analysis in Figure 31, 86.87 % of these sediments in test 1 and 84.25 % in test 2 had particle size 0.125-0.25 mm, representing 2.5-5.0 cm large particles in the prototype.

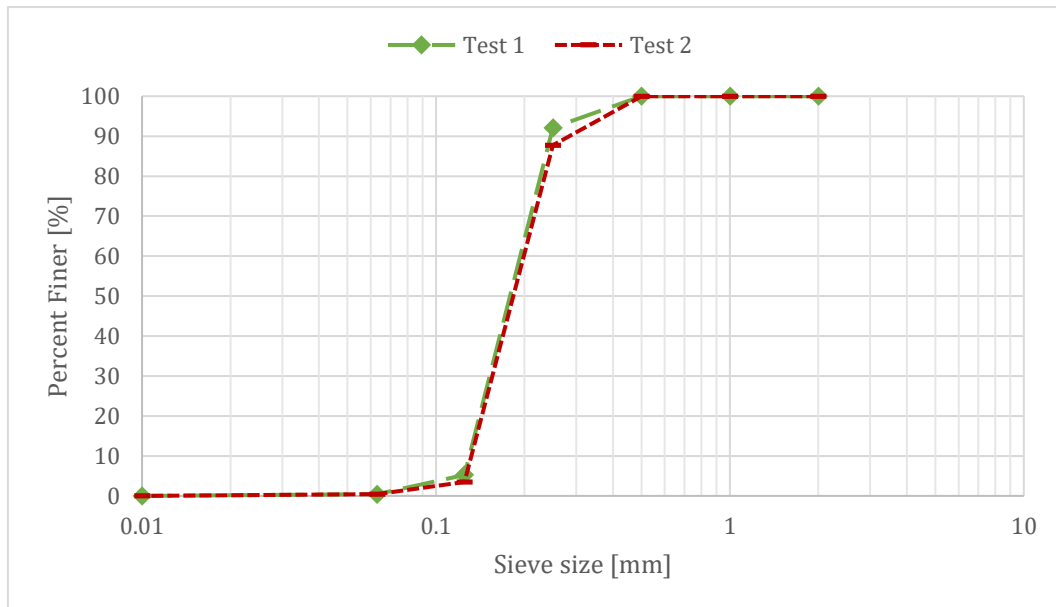


Figure 31 Particle size distribution of sediments collected downstream of the sand trap

Headloss in the sand trap without installed flow calming structures equaled to 4.64 cm for test 1 and 4.77 cm for test 2.

5.1.2 Flow calming structure No. 1

For flow calming structure No. 1, two different approaches of sediments release were tested. In test 3, sediments were delivered to the flume at the water level, while for test 4 the sediments were brought to the bottom which led to different results. One can see in Figure 32 that when delivering the sediments to the water level, sediments needed more time to settle, and therefore they started to settle approximately 0.5 m downstream from the diffuser. Similarly, the sediments covered a bigger area spreading over the entire width of the sandtrap, while in test 4 they were concentrated in the middle of the sand trap, started to settle already in the diffuser and filled the space between individual parts of the flow calming structure, as shown in Figure 33. 1170 grams of sediments were extracted from the flow calming structure representing 9,75 % of all the sediments.

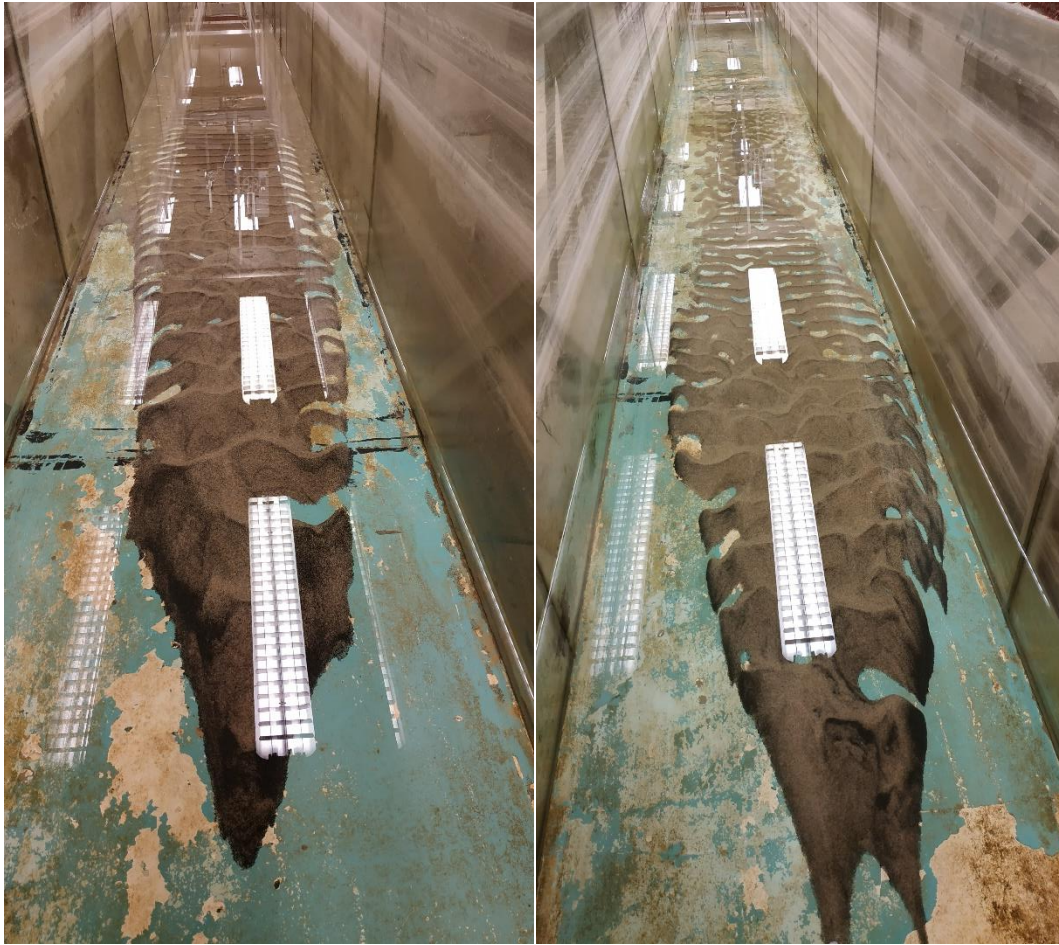


Figure 32 Results from test 3 (on the left side) and test 4 (on the right side) (view from upstream)



Figure 33 Detail of flow calming structure No. 1 after test 4

Since the origin of the sediments in the prototype is mainly material left in the tunnel after its construction, one can assume that sediment transport occurs along the tunnel bottom and therefore all the other experiments were done with sediments brought to the bottom of the flume. For the same reason, the results of test 3 were excluded from this research.

For test 3, sand trap efficiency of 97.63 % was achieved with the total headloss of 9.35 cm whereas, for test 4, the headloss was 9.26 cm and sand trap efficiency equaled to 99.77 %. Sediments not trapped in the sand trap were collected and dried separately, and sieve analysis was done as well. As shown in results of sieve analysis in Figure 34, 88.05 % of these sediments in test 3 and 73.53 % in test 4 had particle size 0.125-0.25 mm, representing 2.5-5.0 cm large particles in the prototype.

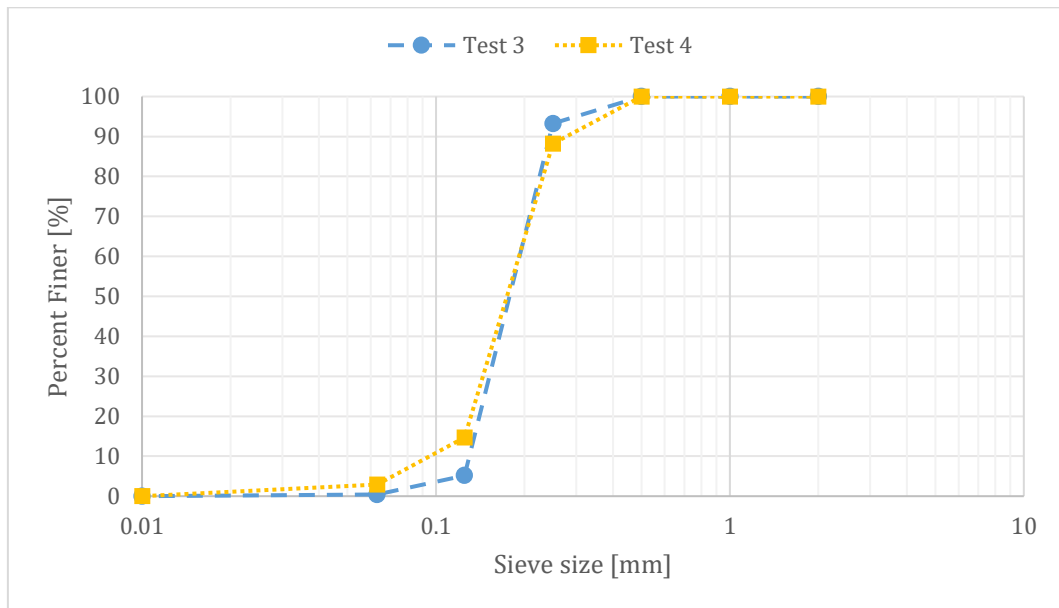


Figure 34 Particle size distribution of sediments collected downstream of the sand trap

Headloss in the sand trap with installed flow calming structures No. 1 was 9.35 cm for test 3 and 9.26 cm for test 4.

5.1.3 Flow calming structure No. 2

For flow calming structure No. 2, tests 5 and 6 were done, and the results of these tests are presented in Figure 35.



Figure 35 Results from test 5 (on the left side) and test 6 (on the right side) (view from upstream)

One could see that the pattern of deposition is the same in both cases. The sediments settled down only in the upstream half of the sand trap creating an approximately 8 cm high deposition of sediments right downstream of the flow calming structure. Detailed side views of these sediment's depositions are shown in Figure 36. Similarly, sediments began to settle down already upstream of the flow calming structure from where 633 grams for test 5 and 610 grams of sediments for test 6 were extracted. These amounts were equal to 5.28 % and 5.08 % of all the sediments, respectively.

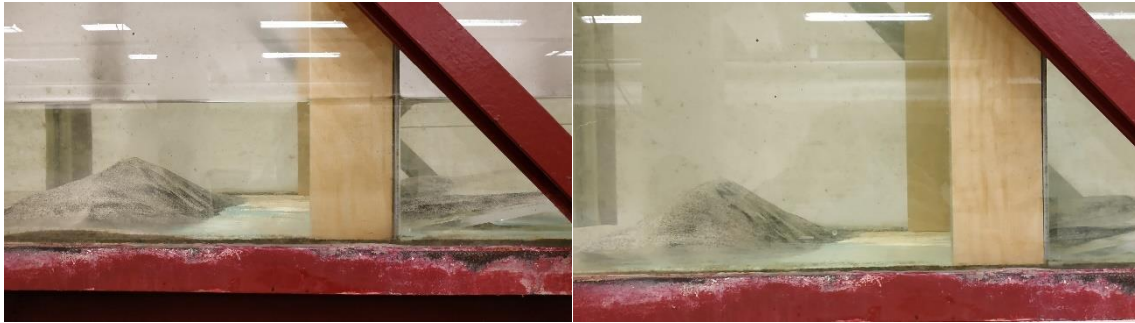


Figure 36 Side view of the sediment's deposition upstream and downstream of the flow calming structure (test 5 on the left side and test 6 on the right side)

From downstream of the sand trap, sediments were extracted only for test 5, and particle size distribution of these sediments is presented in Figure 37. For test 6, no sediments were observed in this location.

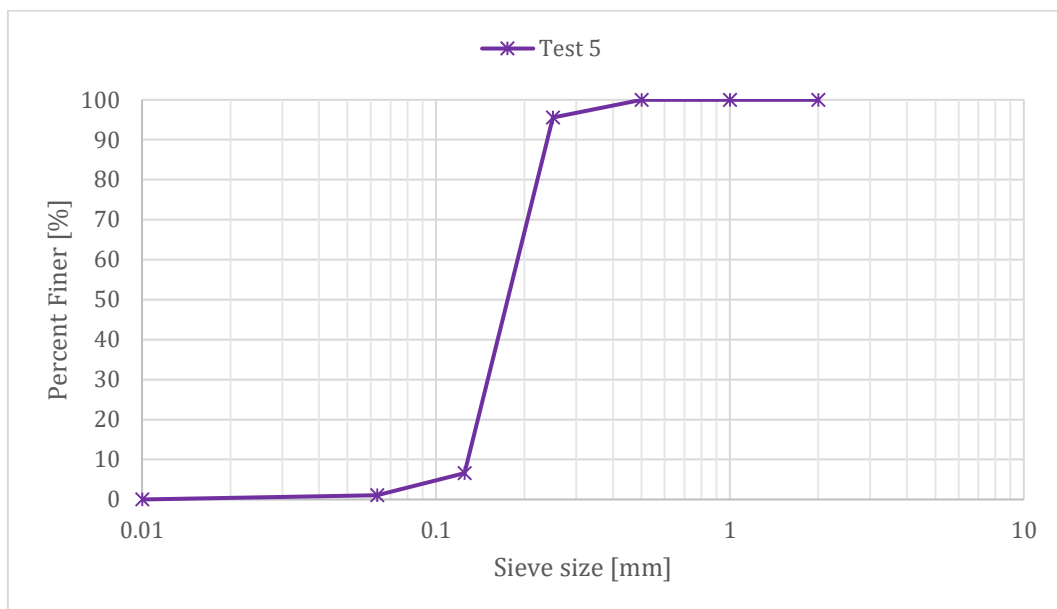


Figure 37 Particle size distribution of sediments collected downstream of the sand trap

Sand trap efficiency for these two tests equaled to 99.19 % and 99.38 % respectively, while the headloss was 24.59 cm for test 5 and 24.44 cm for test 6.

5.1.4 Flow calming structure No. 3

Design of flow calming structure No. 3 allowed to make changes in the arrangement, making it possible to test three different layouts (out of 18 possible layouts). As first, layout 1 with all four rows of rods was tested, and the results of this test are presented in Figure 38.



Figure 38 Results from test 7 (view from upstream)

Particles began to settle right upstream of the structure creating two small depositions of sediments upstream of the last row of rods and one approximately 10 cm high deposition downstream of the structure (Figure 39).



Figure 39 Side view of the sediment's deposition in test 7

Results of all three tests with flow calming structure No. 3 are similar. Particles started to settle already in the diffuser, from where it was extracted 923 g for test 7, 1038 g for test 8 and 790 g of sediments for test 9. The sand trap efficiency for these three tests was 99.69 %, 99.63 %, and 99.96 % respectively. Corresponding values of headloss were 12.51 cm, 6.07 cm, and 8.54 cm.

Results of tests 8 and 9 are presented in Figure 40 and Figure 41.

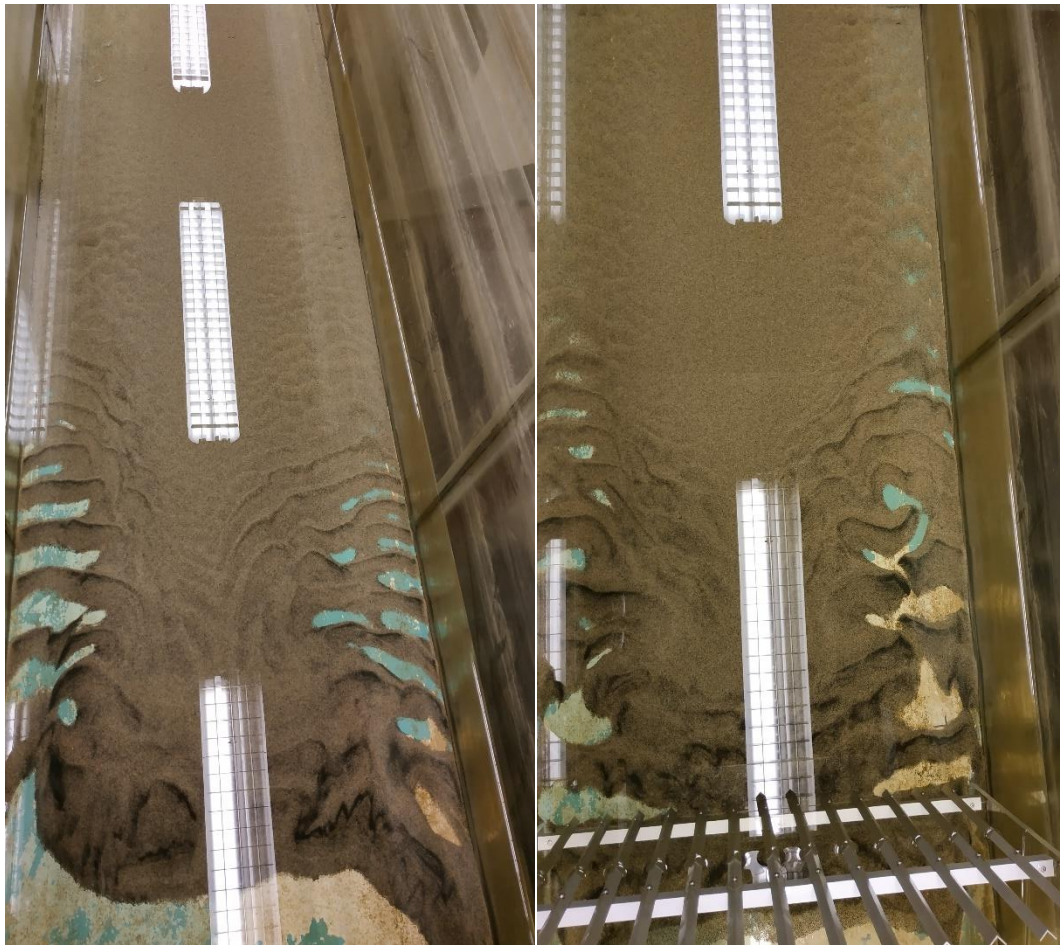


Figure 40 Results from test 8 (on the left side) and test 9 (on the right side) (view from upstream)



Figure 41 Side view of the sediment's deposition (test 8 on the left side and test 9 on the right side)

5.1.5 Comparison of different designs

The three designs of flow calming structures behaved very similarly. Their installation caused that the sediments started to settle earlier, even in the diffuser, and sedimentation occurred only in the upper half of the sand trap. Each of the installed structures increased the sand trap efficiency from 95.67 % on average, to more than 99 %, as shown in Table 2.

Table 2 Overview of results of sand trap efficiency

Type of test	Name	Mass of sediments released to the model [g]	Mass of sediments settled upstream of/in a flow calming structure [g]	Mass of sediments trapped in the sand trap [g]	Mass of sediments collected downstream of the sand trap [g]	Sand trap efficiency [%]
No flow calming structure	Test 1	12000	0	11500	457	95.83
	Test 2	12000	0	11461	489	95.51
Flow calming structure No.1	Test 3*	12000	0	11716	251	97.63
	Test 4	12000	1170	10802	34	99.77
Flow calming structure No.2	Test 5	12000	633	11270	91	99.19
	Test 6	12000	610	11316	0	99.38
Flow calming structure No.3	Test 7	12000	923	11040	0	99.69
	Test 8	12000	1038	10918	0	99.63
	Test 9	12000	790	11205	0	99.96

* Test 3 was excluded from the results because sediments were not released to the bottom of the flume as in the other experiments and therefore behaved differently.

When considering headloss, one can see in Table 3 that each flow calming structure caused different headloss. In the sand trap without any flow calming structure, the headloss equaled to 4.705 mm on average giving headloss of 9.41 cm in the prototype. Installation of the flow calming structures increased the headloss by 1.36–19.89 mm corresponding to 2.72–39.78 cm in the prototype.

Table 3 Overview of results of headloss

Type of test	Name	Water depth upstream of the diffuser [mm]	Water depth on downstream end of the sand trap [mm]	Headloss in the sand trap [mm]	Headloss of the flow calming structure [mm]
No flow calming structure	Test 1	504.25	499.61	4.64	0
	Test 2	503.85	499.08	4.77	0
Flow calming structure No.1	Test 3*	506.21	496.86	9.35	4.64
	Test 4	510.73	501.47	9.26	4.55
Flow calming structure No.2	Test 5	524.16	499.57	24.59	19.89
	Test 6	524.23	499.79	24.44	19.74
Flow calming structure No.3	Test 7	517.36	504.85	12.51	7.80
	Test 8	517.23	511.16	6.07	1.36
	Test 9	513.03	504.49	8.54	3.83

For evaluation of which design is the best, it is important to know the relationship between sand trap efficiency and headloss, when the optimum design causes minimum headloss and secures maximum sand trap efficiency. This is shown in Figure 42.

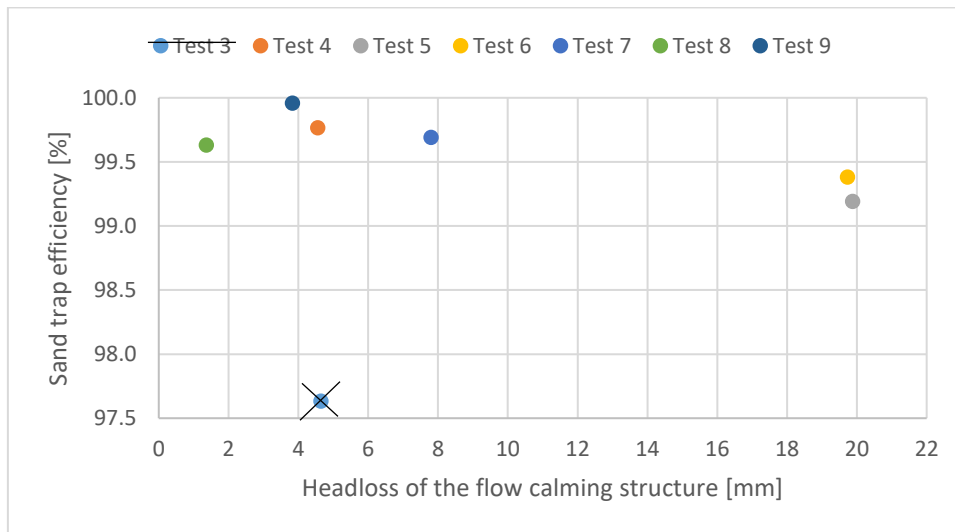


Figure 42 Relationship between sand trap efficiency and headloss caused by flow calming structure

6 Discussion

For flow calming structure No. 1, it was tested to deliver sediments to the flume at the water level (test 3) and to deliver sediments to the flume bed (test 4). In test 4 sediments were deposited already in the diffuser filling the space between individual parts of the flow calming structure, and deposited within the upstream half of the sand trap, while in test 3 sediments needed more time to settle depositing within the whole sand trap with lower sand trap efficiency. In the prototype, sediments have their origin in the material being left in the tunnel after construction, and therefore one can say that bed-load sediment transport occurs in the tunnel. Therefore, results from this experiment were excluded from the research and the other experiments were done with sediments brought to the bottom of the flume. One can say that overall are results from test 4 very promising giving high sand trap efficiency with relatively small headloss.

When testing flow calming structure No. 2, the pattern of deposition was the same in both cases. Approximately 5 % of delivered sediments was trapped upstream of the flow calming structure, and right downstream of this structure an approximately 8 cm high deposition was created. The sediments settled down only in the upstream half of the sand trap with the sand trap efficiency of 99.19 % and 99.38 %, respectively. In contrast to the relatively high efficiency, there was a high headloss compared to the other two designs which make this design least suitable for the implementation in the prototype.

All three tested layouts of flow calming structure No. 3 secured very high sand trap efficiency of 99.69 %, 99.63 %, and 99.96 %, respectively with quite small head loss. Sediments began to settle already upstream of the flow calming structure, creating an approximately 10 cm high deposition right downstream of this structure. This can make it easier to remove deposited sediments from the sand trap.

This master thesis aims to propose an optimum design of flow calming structure to be installed in sand trap 3 in Tonstad HPP. All three designed improved efficiency and shorten the distance needed for particle deposition. Based on testing three different flow calming structures, flow calming structure No. 2 stood out as the least suitable for Tonstad because of its high head loss. On the other hand, flow calming structure No. 1 and No. 3 achieved high sand trap efficiency with smaller headloss than the first mentioned,

however creating a high sediments deposition downstream of the diffuser plays in favor of flow calming structure No. 3.

6.1 Limitation of the study

The main limitation of this study is the use of experimental flume instead of the original sand trap model. While the prototype and the original sand trap model are tunnels with the pressurized flow, all the experiments were done in the channel with an open flow. The differences between pressurized and open channel flow are mainly pressure on the system, shear stress, and velocity profiles. In a tunnel model, pressure in the system can be adjusted to achieve requested velocity. Based on Bernoulli equation, when the static pressure in the tunnel increases, kinetic energy and thus water velocity decreases. For an open channel flow, requested velocity is achieved by using an external source, mostly pump or, as in our case, a propeller installed in a pipe of a closed system.

Even though the cross-sectional area of the sand trap was sufficiently reproduced in the experimental flume, the cross-sectional area upstream of the diffuser was not equal to the one in the original model. Therefore the tested flow calming structures were not completely submerged (Figure 43). This might cause an additional headloss and inaccuracies of the experiments.

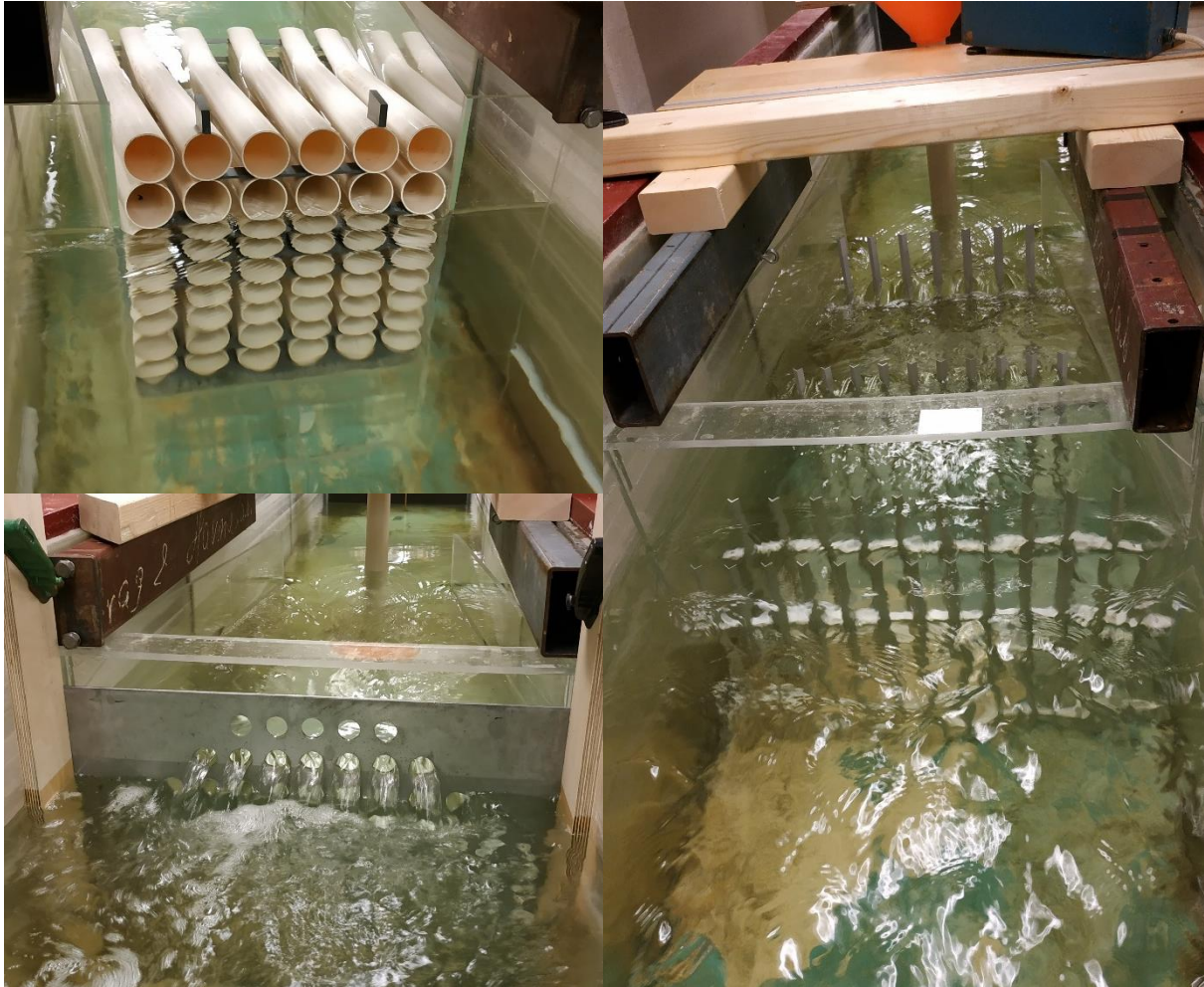


Figure 43 Detail of flow calming structures during the experiments

The flume bed was made up by using various materials like concrete, plexiglass, and plywood. As these materials have different friction, bedload transport might be affected. An even bigger problem than different friction was the current condition of the concrete bed. As shown in Figure 44 the bed was considerably worn out containing many cavities from which it was difficult to extract particles.



Figure 44 Detail of the concrete bed of experimental flume

Another aspect that might affect the results is sediments release. Since in the prototype mainly bed-load sediment transport occurs, it was necessary to bring the sediments to the bed also in the model. Sediment release was done by using a pipe with a diameter of 50 mm. There were three main problems linked to the use of this pipe. Firstly, the pipe created an obstacle in the flow. Secondly, the sediments were released to the model in one point, while in the prototype sediments are entering the diffusor scattered over the entire width. Lastly, the pipe was being clogged with sediments, so it was necessary to clean the pipe several times during the experiment which could affect the results.

Even though there are limitations connected to the type of flow, velocities, different materials in flume bed, these limitations were the same for all the experiments, which make it possible to compare three different flow calming structures to each other.

Errors in the experiment could also be caused by the human factor, for instance when the water depth was measured or when the sediments were extracted from the flume after each test. It could happen that some amount of sediments wasn't removed and affected the following test. Other sources of errors are technical errors caused by equipment used during the experiments, for example, the electric scale used for weighting of sediments, acoustic Doppler velocimeter measuring water velocity or the propeller driving water in the experimental flume.

7 Conclusions

The study presented in this thesis was done as one part of a bigger research project focused on improvements of sand trap 3 of Tonstad hydropower plant. These improvements should reduce the amount of sediments passing the sand trap and subsequently the turbine and thereby reduce operational costs. As described in Chapter 1, the purpose of this master thesis was to design three different flow calming structures, construct them in the model scale, test them in the hydraulic scale model and accordingly propose the optimum design of a sand trap flow calming structure for Tonstad hydropower plant.

Whereas the literature review did not provide enough information on the design of such structures, were they designed based on flow calming structures seen in NTNU's Hydraulic laboratory. Flow calming structures No. 1 and 3 were constructed by the author of this thesis while flow calming structure No. 2 was made with the help of Department of mechanical and industrial engineering at NTNU.

Based on sand trap efficiency, provided all three flow calming structures very similar, satisfactory, results. Sand trap efficiency increased from 95.67 % to more than 99 %, sedimentation began already in the diffuser and occurred mainly in the upstream half of the sand trap. In terms of headloss were the results various. While flow calming structure No. 3, layout 3, increased sand trap efficiency to 99.96 % with a small headloss of 3.83 mm, flow calming structure No. 2 reached sand trap efficiency of 99.19 % with the headloss 5.2 times higher equal to 19.89 mm. This made flow calming structure No. 3 the one to be recommended for further testing and possibly installation in sand trap 3 in Tonstad HPP due to a combination of high sand trap efficiency and small head loss. On the other hand, flow calming structure No. 2 is not recommended.

7.1 Suggestions for future work

Due to complication causing delays of the construction of Tonstad and trap 3 model, the experiments had to be done in another model with open channel flow instead of pressurized flow. Therefore, these experiments should be repeated in the original model when it will be finished, to validate results conducted in this thesis. Redoing the experiments in pressurized flow can also provide information for future experiments if it is possible to obtain the same results in both pressurized and open channel flow.

Similarly, different designs of flow calming structures can be tested to find an optimum design for Tonstad HPP or modification of the designs presented in this thesis can be done. For instance, flow calming structure No. 3 provides in current design 18 different layouts, from which only three were tested in this thesis. At the same time distances between rows and individual rods can be extended/reduced. Since in this thesis, as rods were used L profiles with an angle of 90° , one can see an option in use of profiles with an angle other than 90° .

8 References

- Armaroli, N., & Balzani, V. (2007). The future of energy supply: challenges and opportunities. *Angewandte Chemie International Edition*, 46(1-2), 52-66.
- Bartholdy, J., Ernstsens, V. B., Flemming, B. W., Winter, C., Bartholomä, A., & Kroon, A. (2015). On the formation of current ripples. *Scientific reports*, 5, 11390.
- Bilgen, S., Kaygusuz, K., & Sari, A. (2004). Renewable energy for a clean and sustainable future. *Energy sources*, 26(12), 1119-1129.
- Brevik, O. (2013). *3D NUMERISK MODELLERING AV DELER AV VANNVEGEN TIL TONSTAD KRAFTVERK*. Institutt for vann-og miljøteknikk,
- Buckingham, E. (1914). On Physically Similar Systems; Illustrations of the Use of Dimensional Equations. *Physical Review*, 4(4), 345-376.
- Chow, V. T. (1959). Open channel flow. *London: McGRAW-HILL*, 11(95), 99,136-140.
- Dey, S. (2014). Bed-Load Transport. In *Fluvial Hydrodynamics*. Berlin, Heidelberg: Springer.
- Dincer, I. (2001). Environmental issues: li-potential solutions. *Energy sources*, 23(1), 83-92.
- Douglas J. F., G. J. M., Swaffield J. A., Jack L. B. (2011). *Fluid mechanics* (6th ed.). New York: Prentice Hall.
- Ettema, R., Arndt, R., Roberts, P., & Wahl, T. (2000). *Hydraulic modeling: Concepts and practice*.
- Julien, P. Y. (2010). *Erosion and sedimentation*: Cambridge University Press.
- Killingtveit, Å. (2019). Hydropower. In *Managing Global Warming* (pp. 265-315): Elsevier.
- Lia, L., Jensen, T., Stensby, K., Midttomme, G., & Ruud, A. (2015). The current status of hydropower development and dam construction in Norway. *Int. J. Hydropower Dams*, 3, 37-43.
- Lysne, D. K., Glover, B., Støle, H., & Tesaker, E. (2003). *Hydraulic design*: Norwegian University of Science and Technology, Department of Hydraulic and
- Michaelides, E. E. S. (2012). *Alternative energy sources*: Springer Science & Business Media.
- NTH. (1967). *Tonstad kraftverk: Sandfang- og strømningsundersøkelser*. Retrieved from Trondheim:
- Open channel flow. Flow tranquilizers/conditioners for flumes. Retrieved from <https://www.openchannelflow.com/blog/flow-tranquilizers-conditioners-for-flumes>
- Paschmann, C., Fernandes, J. N., Vetsch, D. F., & Boes, R. M. (2017). Assessment of flow field and sediment flux at alpine desanding facilities. *International Journal of River Basin Management*, 15(3), 287-295.
- Patel, M. R. (2005). *Wind and solar power systems: design, analysis, and operation*: CRC press.
- Shields, A. (1936). Application of similarity principles and turbulence research to bed-load movement.
- Sira-Kvina Kraftselskap. Tonstad kraftverk. Retrieved from <https://www.sirakvina.no/tonstad-kraftverk/tonstad-kraftverk-article260-919.html>
- Sira-Kvina Kraftselskap. (2016). *Design basis: Sand Trap 3 - Physical Scale Model*. Retrieved from

8 References

- SITEC. Sandabzugssystem HSR. Retrieved from <https://www.sitec.hsr.ch/Sandabzugssystem-HSR.14763.0.html>
- Steinkjer, S. M. (2018). *Hydraulic scale modeling of sediments for pressurized sand traps*.
- Tracom fiberglass products. The Best Way to Condition Flow in Flumes. Retrieved from <https://tracomfrp.com/best-way-condition-flow-flumes/>
- Vereide, K., Svingen, B., & Guddal, R. (2015). Case study: Damaging effects of increasing the installed capacity in an existing hydropower plant.

9 Appendices

Appendix A: Drawings of the prototype

